International Journal Of Remote Sensing
March 2016, Volume 37 Issue 5 Pages 1089-1114
http://dx.doi.org/10.1080/01431161.2016.1145362
http://archimer.ifremer.fr/doc/00319/42986/

Assessment of seasonal and year-to-year surface salinity signals retrieved from SMOS and Aquarius missions in the Bay of Bengal

Akhil V. P. [1, *], Lengaigne Matthieu [2, 3, 5], Durand Fabien [1], Vialard Jerome [3, 5], Chaitanya A. V. S. [4], Keerthi M. G. [2], Gopalakrishna V. V. [4], Boutin Jacqueline [3, 5], De Boyer Montegut Clement

[1] IRD, LEGOS, Toulouse, France.
[2] NIO, Indofrench Cell Water Sci, IISc NIO IITM IRD Joint Int Lab, Panaji, Goa, India.
[3] Univ Paris 06, Univ Paris 04, LOCEAN IPSL, CNRS IRD MNHN, Paris, France.
[4] NIO, Panaji, Goa, India.
[5] IFREMER, LOS, Plouzane, France.

* Corresponding author : V. P. Akhil, email address : akhil1585@gmail.com

Abstract :

The Bay of Bengal (BoB) exhibits a wide range of sea surface salinity (SSS), with very fresh water induced by heavy monsoonal precipitation and river run-offs to the north, and saltier water to the south. This is a particularly challenging region for the application of satellite-derived SSS measurements because of the potential pollution of the SSS signal by radio frequency interference (RFI) and land-induced contamination in this semi-enclosed basin. The present study validates recent level-3 monthly gridded (1° × 1°) SSS products from Soil Moisture and Ocean Salinity (SMOS) and Aquarius missions to an exhaustive *in situ* SSS product for the BoB. Current SMOS SSS retrievals do not perform better than existing climatologies. This is in stark contrast to Aquarius, which outperforms SMOS and available SSS climatologies everywhere in the BoB. While SMOS only captures the SSS seasonal evolution in the northern part of the Bay, Aquarius accurately captures the seasonal signal in the entire basin. The Aquarius product is also able to capture SSS non-seasonal anomalies, with an approximate correlation (*r*) of 0.75 with box-averaged *in situ* data in the northern, central, and western parts of the Bay. Aquarius can, thus, be confidently used to monitor large-scale year-to-year SSS variations in the BoB.

1. Introduction

The Bay of Bengal (BoB) stands out as a very peculiar region for salinity distribution in the tropical belt. The strong summer monsoon oceanic rainfall and continental runoffs into this relatively small and semi-enclosed basin result in an intense dilution of the seawater in northern part of the Bay, therefore inducing some of the lowest sea surface salinity (SSS) in the tropical belt (Figure 1). The resulting very strong near-surface salinity vertical stratification is believed to play a key role in the regional climate (Shenoi *et al.* 2002, Neetu *et al.* 2012). Indeed, the enhancement of near-surface ocean stability by salinity stratification reduces turbulent entrainment of cooler thermocline water into the mixed layer and consequently maintains high sea surface temperatures in the BoB (Shenoi et al. 2002). The stronger BoB salinity stratification after the monsoon may also favour intense cyclones during that season, by inhibiting oceanic vertical mixing and surface cooling along the cyclone track, and hence leading to enhanced evaporation that can sustain the cyclone (Neetu *et al.* 2012 and references therein). Last but not least, salinity could also act as a marker of changes in the water cycle associated with anthropogenic forcing (e.g. Terray *et al.* 2012).

Because of the potentially important role of salinity in the climate dynamics of this region, several studies already investigated the seasonal BoB SSS variations by building salinity climatologies derived from available hydrographic data (e.g. Rao and Sivakumar. 2003, Chatterjee *et al.* 2012, Zweng *et al.* 2013), These climatologies reveal a strong freshening in the northeastern part of the Bay during summer in response to the freshwater input associated with monsoonal rainfall and Ganges-Brahmaputra river discharge (Figure 1*a*). This freshwater pool further strengthens and expands southward along the eastern and western boundaries of the Bay in fall (Figure 1*b*). It then weakens during winter (Figure 1*c*) and retreats back to the northeasternmost part of the Bay during spring (Figure 1*d*). While these climatologies are not able to capture the fine spatial scale of this coastal freshening (Chaitanya *et al.* 2014a), the coverage of in situ data used in these products is sufficient to capture the main large-scale SSS seasonal features in the Bay (Chatterjee *et al.* 2012). The monitoring of the year-to-year SSS variability is however generally far more challenging due to the insufficient spatio-temporal sampling by the in situ network (Vinayachandran and Nanjundiah 2009, Chaitanya *et al.* 2014b).

The advent of satellite salinity measurements provides a unique opportunity to improve the monitoring of SSS variations in this climatically relevant region. The Soil Moisture and Ocean Salinity (SMOS) European mission (Mecklenburg *et al.* 2008) launched in November 2009 and the Argentina/US Aquarius mission (Lagerloef *et al.* 2008) from June 2011 to June 2015 both provide global SSS estimates. These new spaceborne SSS measurements have been routinely validated, with global root-mean-square errors around 0.2 practical salinity scale (pss) for monthly Aquarius SSS fields around 150 km × 150 km global grid (Lagerloef *et al*. 2013) and for 10-days SMOS averages around 100 km × 100 km grid in the tropical regions (Boutin *et al*. 2012). Recent research has demonstrated the value of these satellite missions in capturing open-ocean signals related to large-scale climate modes such as La Niña signature in the tropical Pacific (Hasson *et al.* 2014), the Indian Ocean Dipole signature in the eastern part of the equatorial Indian Ocean (Durand *et al.* 2013) or planetary waves signature in the Southern Indian Ocean (Menezes *et al.* 2014). The assimilation of Aquarius SSS also improves the simulation of the equatorial Wyrkti jets in the Indian Ocean (Chakraborty *et al*. 2014).

Whether these satellite data can accurately capture SSS variations in relatively small basins surrounded by continental masses however remains unclear. Near-coastal environments are indeed particularly challenging for the application of satellite-derived SSS measurements because radio frequency interferences (RFI) linked to artificial sources (e.g. radars that emit in the frequency band of the instruments) and land-induced contamination on antenna side lobes (Reul *et al.* 2012, Subrahmanyam *et al.* 2013) can obscure climatically relevant signals. A recent study (Gierach *et al.* 2013) however demonstrated the ability of both Aquarius and SMOS to monitor SSS variations in the Gulf of Mexico, offering promises for monitoring SSS evolution in a near-coastal environment.

The BoB, approximately 1000-2000 km wide semi-enclosed basin similar to the Gulf of Mexico, is also very challenging for SSS satellite retrievals. A thorough validation of the SSS remotely-sensed products is therefore a pre-requisite before using these data to describe and understand the SSS evolution in this region. Preliminary analyses reported major issues in the satellites ability to retrieve SSS there. Subrahmanyam *et al.* (2013) and Ratheesh *et al.* (2013) indeed reported an erratic behaviour of an earlier version of the level-3 SMOS dataset used in the current study for that region for the year 2010, with weak and insignificant spatial correlations, and attributed this behaviour to RFI and land contamination. Similarly, analyses performed by Ratheesh *et al.* (2014) for level-3 Aquarius dataset over the entire Indian Ocean region from August 2011 to December 2012 reported a 0.5 pss overestimation and a poor agreement with observations for SSS values lower than 32 pss, which are typical of the northern part of the BoB.

While the above analyses revealed a poor accuracy of the preliminary satellite retrievals of the Bay of Bengal SSS, recent evolutions such as an improved roughness correction for Aquarius (Yueh *et al.* 2014) and an improved handling of RFI contamination for SMOS (Reul *et al.* 2014) are now available for the most recent SSS products derived from the satellites microwave measurements. In addition, both missions have now accumulated about three years of data, allowing a qualitative assessment of the ability of each satellite to capture the seasonal and year-to-year SSS evolution in this region. The goal of the present study is therefore to provide an in-depth, up-to-date assessment of the ability of both satellites to monitor the seasonal and year-to-year SSS variations in the BoB. This will be done by splitting the basin into various sub-regions and by comparing remotely-sensed SSS to a comprehensive dataset compiling all in situ observations available during the recent period (Chaitanya *et al.* 2014b). This paper will focus on the validation of the most recent versions (at the time of writing) of monthly level-3 products for both missions. Due to the larger number of measurements used to compute the SSS pixel-average, these monthly resolution products are indeed expected to exhibit a better accuracy compared to products derived at a higher temporal resolution from the same data and methods (Hernandez *et al.* 2014).

2. Datasets and methods

This section describes the two satellite SSS products (Sections 2.1 and 2.2), the in situ dataset (Sections 2.3) used in the present study and discusses the co-location method used to compare in situ and remotely sensed data (Section 2.4).

2.1 SMOS level-3 data

SMOS is a polar orbiting satellite with a passive microwave sensor operating within the L-Band (at 1.404-1.423 GHz), operated as part of European Space Agency (ESA)'s Living Planet Programme (McMullan *et al.* 2008, Mecklenburg *et al.* 2012). SMOS was launched on 2 November 2009, making it the first satellite to provide continuous multi-angular L-band radiometric measurements over the globe. It is based on 69 individual radiometers that are used to retrieve the SSS field through polarimetric interferometry (see Kerr *et al.* 2010, Reul *et al.* 2012, 2013, and references therein for further details on the measurement technique). Due to the interferometry principle and the antenna shape, the field of view is 1200 km wide and a global coverage is achieved every three days.

Instantaneous SSS retrievals under the satellite swath, corresponding to ESA level-2 SSS products, have a spatial resolution of 43 km but a rather low accuracy of 0.6 to 1.7 pss (Reul *et al.* 2012, Boutin *et al.* 2012). After averaging these measurements over one month, 100 km, and after removing large-scale biases, the level-2 version 5 processor provided by CATDS/LOCEAN expertise center (available at www.catds.fr) achieve an accuracy of 0.2-0.3 pss in subtropical regions free of RFIs (Hernandez *et al.* 2014, Hasson *et al.* 2014). Unfortunately, the procedure of outliers and RFI sorting used in this dataset flags almost all the SMOS measurements in the BoB as bad data. Hence, in this study, we use the 1°×1° gridded monthly SSS composites from the V02 version of the SMOS level-3 research product generated by the CATDS/Ifremer expertise center (also available at www.catds.fr). With respect to the ESA level 2 processing, it includes an improved RFI mitigation and a 5°×5° adjustment to the World Ocean Atlas SSS climatology of Antonov *et al.* (2010) to remove residual temporal drifts and land contamination in SMOS brightness temperature level 1 products (Reul *et al.* 2014). This SSS bias mitigation and the improved RFI handling enhance the data quality close to the coast compared to other level-3 products (Zhang *et al.* 2013).

Data of the first four months of 2010 were not reprocessed because of reduced data quality during that period. This product therefore covers the May 2010-December 2013 period. As shown on Figure 2*a*, this product has few missing values throughout the central and southern Bay. The percentage of valid data however drops considerably in the northeastern part of the basin near the Ganges-Brahmaputra river mouth, with any SSS retrieval north of 20°N. This drop largely results from brightness temperature data flagged as outliers (not shown).

2.2 Aquarius level 3 data

Aquarius is NASA's Earth orbiting mission launched on 10 June 2011. The Aquarius instrument measures the brightness temperature of the sea surface within the L-band (1.400-1.427 GHz) with three separate radiometers and the surface roughness with an active scatterometer operating at 1.2 GHz. These data, in combination with concurrent SST, and other auxiliary data, are used to estimate SSS. The resolution of individual SSS measurements is 100-150 km and a global coverage of the ocean is obtained after about 7 days. After four years of successful data collection this mission ended on 7 June 2015 due to an unrecoverable hardware failure.

This study uses the CAPv3 Aquarius level-3 1°×1° monthly composites. This product combines the measurements from the three radiometers and the scatterometer using the Combined Active-Passive Algorithm applied to version 3.0 of the Aquarius/SAC-D data updated in July 2014 (available at ftp://podaac-ftp.jpl.nasa.gov/allData/aquarius/L3/mapped/CAPv3). This algorithm computes SSS by minimizing the least squares error between measurements and model functions of brightness temperatures and radar backscatter. It also includes a rain-corrected salinity based on collocated SSMI/S and WindSAT data. This rain correction algorithm has been established assuming that the freshwater inputs are homogeneously spread over the first 5 m and hence, in case of rain-induced surface fresh cells, it is expected to overestimate the SSS (Tang *et al.* 2014).

This product covers the August 2011 - June 2014 period. Like SMOS (Figure 2*a*), Aquarius exhibits few missing data south of 15°N (Figure 2*b*). However, Aquarius offers a better spatial coverage in the northernmost part of the basin as compared to SMOS, because there is no far-reaching RFI issue for Aquarius whose antenna lobes are much narrower than for SMOS, due to the interferometry technique used for the SMOS instrument.

2.3 North Indian Ocean Atlas climatology

The recent North Indian Ocean Atlas (NIOA) SSS climatology issued by Chatterjee *et al.* (2012) and shown in Figure 1 is used to qualitatively validate the SSS seasonal cycle from the satellite data. This 1°×1° monthly climatology includes all the data from the World Ocean Database 2009 (WOD09) (Locarnini *et al.* 2010, Antonov *et al.* 2010), complemented with Conductivity-Temperature-Depth (CTD) stations from Indian oceanographic cruises. The inclusion of the Indian oceanographic cruises database in NIOA considerably improves the data coverage in the periphery of the BoB compared with WOD09, especially along its western boundary (Chatterjee *et al.* 2012). Year-to-year SSS anomalies from both satellite datasets and in situ products detailed below are calculated by subtracting this NIOA climatology from their raw values.

2.4. Blended in situ dataset

2.4.1 Data sources

Comparisons with a recent in situ dataset directly derived from the one presented in Chaitanya *et al.* (2014b) will allow a quantitative validation of the satellites retrieval. This dataset compiles all the available in situ SSS measurements over the BoB from December 2008 to June 2014. It gathers six different salinity data sources: Array for Real-Time Geostrophic Oceanography (Argo) profilers (Roemmich *et al.* 2009), ship-of-opportunity eXpendable Conductivity-Temperature-Depth (XCTD) profiles and bucket measurements (Chaitanya *et al.* 2014a), Research Moored Array for African-Asian-Australian Monsoon Analysis and Prediction (RAMA) moorings (McPhaden *et al.* 2009), Ocean Moored buoy

Network for Northern Indian Ocean (OMNI) moorings (Venkatesan *et. al.* 2013), ship-of-opportunity thermosalinograph transects (Alory et al., 2015) and dedicated hydrographic cruises. Argo profiles are the main contributor to this SSS product. Considering the uppermost valid measurements within the 5 m to 15 m layer, typically located at around 8 m depth, there are more than 10000 valid salinity measurements over the 2009-2014 period. This in situ dataset also includes 1200 valid measurements at about 1 m depth from bucket samples and at about 5 m depth from XCTD salinity measurements collected on an approximately bimonthly basis along two repeated merchant ship tracks between Chennai (label ‘ C ’ in Figure 2*c*,*d*) and Port Blair (label ‘ PB ’), and between Kolkata (label ‘ K ’) and Port Blair. In addition, our dataset comprises point-wise salinity measurements at 1 m depth over the 2009-2014 period from three RAMA moorings (90°E-8°N; 90°E-12°N and 90°E-15°N; circles on Figure 2*c*,*d*) and at 5 m depth from six OMNI moorings (86°E-11°N, 85°E-8°N, 83°E-14°N, 88°E-16°N, 94°E-10°N, 89°E-18°N; triangles on Figure 2*c*,*d*). Finally, this dataset also includes salinity measurements representative of the 0-10 m upper ocean layer derived from a thermosalinograph on-board a merchant ship (M/S Lavender) crossing the southern Bay every 3-4 months during the October 2008 to October 2012 period (dotted line in Figure 2*c*,*d*) and a few 0-10 m depth measurements from shipborne CTD casts in the coastal western Bay provided by the National Institute of Oceanography Data Centre (India).

2.4.2. Colocation method

In a similar way to Chaitanya *et al.* (2014b), these six data sources were merged into a single dataset by computing the median of all available individual measurements (irrespective of their nature: autonomous profiler, mooring, underway ship measurements), at the spatial and temporal resolution of the satellite products (1°×1°×1 month).

The gridding is performed on both the SMOS and AQUARIUS native 1°×1° grids which are offset by 0.5° both in latitude and in longitude, resulting in two versions of our gridded product. The main difference with the original in situ product presented in Chaitanya *et al.* (2014b) is the temporal resolution: while Chaitanya *et al.* (2014b) used a product with a 3 months temporal resolution, the present study uses a monthly resolution to allow a validation of the both satellites level-3 monthly products.

Figure 2*c*,*d* illustrates the data density of the in situ data, collocated with each of the remotely-sensed SSS products. The in situ validation data density is rather heterogeneous, with a reasonably good sampling over most of the central part of the Bay but sparser data in near-coastal regions. This analysis also reveals that the Andaman Sea (east of 93°E and south of 15°N) is practically devoid of in situ observations, preventing an assessment of the remotely sensed SSS products there.

In the following, a detailed description of the SSS variability in the BoB will be inferred by dividing the domain into four coherent sub-regions outlined on Figure 2*e*,*f*. The first sub-region covers the northern part of the basin (NBoB, 86°E-94°E; 16°N-23°N) where the largest SSS fluctuations are found, due to both the proximity of the Ganges-Brahmaputra river mouths and monsoonal precipitation (Rao and Sivakumar 2003, Akhil *et al.* 2014). The second sub-region is located in the western part of the Bay (WBoB, 80°E-84°E; 6°N-16°N) and encompasses the coastal region through which the NBoB freshening is transported southward during winter as a fresh tongue hugging the eastern Indian coastline (Chaitanya *et al.* 2014a, Akhil *et al.* 2014). A third sub-region is located in the central BoB (CBoB, 84°E-94°E; 6°N-16°N), where the SSS variability is known to be weaker. Finally, a fourth sub-domain is considered in the Andaman Sea (94°E-99°E; 6°N-18°N), where the variability derived from satellite products is about as strong as in the northern part of the basin (Figure 2*e*,*f*) but cannot be validated due to the lack of in situ observations (Figure 2*c*,*d*). We will compare the remotely-sensed SSS to in situ data on their 1°×1° monthly native grids, but also from averages over the boxes above. This spatial averaging has the advantage of smoothing out representation error of the in situ data, potential noise in the satellite retrievals, and to focus the comparison with in situ data on large-scale features.

2.4.3 Estimation of the accuracy of the in situ gridded SSS product

As our SSS gridded products will serve as references for the SMOS and Aquarius validation, this subsection provides a discussion of the accuracy of this new observational dataset. Subrahmanyam et al. (2013) reported that the instrumental error of ARGO is lower than 0.01 pss. This is also the typical instrumental accuracy of bucket measurements, RAMA moorings and thermosalinograph transects. This instrumental error is completely negligible compared with the representation error (i.e. the error on the 1° × 1° × 1 month average SSS estimate due to an incomplete sampling of this spatio-temporal domain, Delcroix et al., 2005) and will not be further discussed.

Argo, CTD and thermosalinograph salinity measurements used in our in situ reference datasets are not collected right at the surface, but are rather representative of the 5-10 m depth layer. Owing to the strong haline stratification, especially in the northern Bay of Bengal, there may be an error on the surface salinity estimate resulting from this deeper measurement depth. This error can be estimated from the data provided by the three RAMA moorings at 90°E15°N, 90°E12°N and 90°E8°N. These moorings indeed provide simultaneous daily salinity measurements at 1 m and 10 m depth for one to two years, depending on the site. The scatterplot between those 1 m and 10 m depth salinity measurements on Figure 3 highlights the very good coherency between the variability inferred from these two depths, with a correlation exceeding 0.97 at the three moorings location. As expected, the salinity at 10 m (a typical sampling depth for the nearest measurement to the surface for Argo profiles) is on average saltier by 0.06 pss than the 1 m salinity at the northernmost mooring. This mean difference is negligible at the two moorings further south, where the stratification is not as strong as in the northern BoB. The larger mean bias (0.06 pss) and slightly weaker correlation (0.97) between 1 m and 10 m measurements at the northernmost mooring results in a larger root mean square error (RMSE) there (0.19 pss) as compared to the other moorings further south (around 0.07 pss). A 0.2 pss RMSE is about ten times smaller than the SSS variations in our in situ blended product (STD of 2.14 pss). We will also see in Section 3 that this error is four times weaker than the typical RMSE of the SMOS or Aquarius products. This suggests that the varying depth of salinity data collection will not heavily affect our assessment of the satellite SSS products.

SSS in the BoB varies a lot both spatially (filaments generated by the stirring from meso-scale eddies, localized rain…) and temporally, with large SSS changes over short periods and/or short space scales (Benshila et al., 2014, and references therein). Most 1° × 1° × 1 month reduced SSS estimates from our blended product only use 1 to 10 individual observations, with a median of 2 (not shown). The median of such a small number of point-wise observations may not be representative of the actual monthly mean SSS in the 1° × 1° pixel. Figure 4 provides an estimate of this representation error. We took advantage of the relatively large number of daily observations at RAMA moorings (about 30 per month), in order to estimate the impact of the number of available observations on the accuracy of the estimate of the monthly 1° × 1° SSS average. The underlying hypothesis is that the 30 daily-sample average of RAMA is representative of the 1° × 1° × 1 month pixel. We perform a random subsampling of N daily 1 m salinity measurements from RAMA moorings each month, with N ranging from 1 to 15. We repeat this random subsampling 1000 times: figure 4 shows the RMSE and correlation of the subsampled estimate against the actual monthly value, as a function of the number of available observations *N*.

For the three moorings, the correlation exceeds 0.95 and RMSE is lower than 0.1 pss if more than 10 observations are available. As expected, this correlation decreases and the RMSE increases as the number of available observations decreases. The median value of the number of observations in each 1° × 1° × 1 month cell in our reference in situ dataset is 2. This results in a correlation of about 0.92 and RMSE about 0.18 pss for the moorings located in the central and southern part of the basin, and 0.84 / 0.3 pss for the northernmost mooring. We can therefore consider a root mean square representation error of 0.3 pss for our-in situ dataset. As a result, the assessment of SMOS and AQUARIUS datasets will only be possible up to this level of accuracy. This 0.3 pss value is however still far lower than the SSS variations in our gridded in situ and we will see that it is less than half of the estimated RMSE of individual pixels from satellite products. As mentioned earlier, we will also compare our in situ dataset with satellite data over larger boxes to further reduce the impact of this representation error.

3. General evaluation of the remotely-sensed SSS products

Figure 5 can be inserted here

Figure 5*a*,*b* provides a synthetic view of the consistency between the 1°×1° monthly remotely-sensed SSS estimates and the in situ reference product. These panels illustrate that the phase agreement with in situ dataset is generally better for Aquarius (0.82 correlation) as compared to SMOS dataset (0.69 correlation). In addition, Aquarius does not exhibit any significant basin-scale SSS bias (0.01 pss), while SMOS generally underestimates the SSS in the BoB (-0.22 pss). The SMOS and Aquarius estimated RMSE (approximately 0.9 pss) largely exceeds the uncertainties derived for the in situ product (0.1-0.2 pss attributable to the different sampling depth and 0.2-0.3 pss for the spatio-temporal representation error). Rather surprisingly, Aquarius however exhibits the same RMSE as SMOS (around 0.88 pss). Those statistics are however computed over different subset of the whole in situ dataset, due to the different periods, grids and missing data areas of the two satellite products. We thus re-computed the above statistics for the same sample (i.e. common pixels for the SMOS, Aquarius and reference in situ product; numbers in brackets on Figure 5*a*,*b*) to allow a fair comparison between the two satellite products. This reveals that Aquarius outperforms SMOS retrieval for all considered statistics. The Aquarius RMSE, in particular, is 0.68 pss and smaller than SMOS (0.89 pss) when considering the sample common to the three products. This sensitivity of Aquarius RMSE to the collocation method (0.68 pss for the common sample and 0.88 pss for the in situ – Aquarius collocated data) arises from the extended Aquarius coverage that allows retrieving SSS in the northern part of Bay, which is not the case for the SMOS product (Figure 2*a*,*b*). The northern Bay of Bengal displays an intense fine-scale and high-frequency SSS variability due to stirring of intense SSS gradients by meso-scale eddies (Benshila et al., 2014, and references therein). The relatively large RMSE of Aquarius in the Northern BoB is thus likely related to the Aquarius / in situ validation dataset inability to properly capture small-scale variability in this region (illustrated by the larger scatter between Aquarius and in situ data for low SSS values, Figure 5*b*). A closer look at Figure 5*a*,*b* also reveals that the satellites performance strongly varies depending on the SSS value. While Aquarius does not show any significant bias for SSS ranging from 34 to 31 pss, SMOS is generally fresher than the reference product for SSS higher than 33 pss and saltier for SSS lower than 33 pss. The scatter of both satellites around the reference value is also particularly large for the NBoB box (blue dots on Figure 5*a*,*b*) compared to the other regions.

Aside from an inaccurate SSS retrieval, small spatial scale and high frequency SSS features sampled by in situ observations but not by the satellite products may account for some of the inconsistencies between in situ and satellite measurements, as discussed in previous section. Comparing spatial averages of these three datasets over the large boxes presented in Section 2.4 allows to smooth out a large part of small scale SSS variations in the in situ datasets and noise in the satellite data retrieval and therefore to assess the impact of small spatial scale and high frequency features on our SSS validation. The results are presented on Figure 5*c,d*. Both SMOS and Aquarius correlations increase by about 0.1 when considering box-averaged values rather than pixel-wise. The RMSE reduction is however larger for Aquarius (from 0.88 pss to 0.49 pss) than for SMOS (from 0.88 pss to 0.63 pss). This larger error reduction in Aquarius suggests that part of the mismatch between Aquarius and in situ data is attributable to small-scale spatial noise smoothed out when averaging over a large box (typically 1000 km wide) while a larger part of the SMOS retrieval error has probably a broader spatial scale, and hence cannot be reduced by spatial averaging.

Figure 6 further provides a synthetic assessment of the ability of both satellites to retrieve the SSS in the NBoB, WBoB and CBoB sub-regions. It features the bias, correlation and RMSE between box-averaged satellite and in situ values. As far as the mean state is concerned, SMOS retrievals exhibit a systematic fresh bias everywhere in the Bay (Figure 6*a*), ranging from -0.19 pss in WBoB to -0.35 pss in NBoB. This result is opposite to Reul *et al.* (2012) and Ratheesh *et al.* (2013) who both reported a salty bias of SMOS retrievals over the Bay over the year 2010. In contrast, Aquarius exhibits a bias weaker than 0.1 pss in CBoB and WBoB and a fresh bias of -0.26 pss in NBoB (Figure 6*a*). The phase agreement is also considerably better for Aquarius than for SMOS in all sub-regions: Aquarius correlations range from 0.79 in WBoB to 0.94 in NBoB while SMOS correlations are considerably weaker, ranging from 0.24 in WBoB to 0.69 in NBoB (Figure 6*b*). Aquarius also outperforms SMOS in all BoB sub-regions when considering the RMSE statistics (Figure 6*c*).

The above analyses show that Aquarius outperforms SMOS for all statistics and all sub-regions of the BoB. SMOS appears to be particularly poor in retrieving the SSS variability in the central and western part of the BoB (correlations inferior to 0.4) while Aquarius performs satisfactorily over the entire BoB (correlations of order or larger than 0.8). The SSS variability in each sub-region can arise either from seasonal variations or from departures from the climatological seasonal cycle. The next two sections provide a validation of both satellites at these two timescales.

4. Evaluation of SSS seasonal evolution

Figure 7 displays the NIOA quarterly climatology, along with the corresponding climatology derived from SMOS and Aquarius. Of course, the three products are not expected to be strictly comparable, because SMOS and Aquarius measurements cover a much shorter period than those gathered in the NIOA. This figure hence only provides a qualitative assessment of the remotely-sensed SSS spatial distribution. A more quantitative validation of the seasonal SSS evolution of satellite data against in situ measurements will be presented in Figure 8.

As already mentioned in the introduction, there is a strong contrast between fresh waters to the northeast and saltier waters in the southwestern part during the monsoon (Figure 7*a*). Highest SSS values (>34 pss) are found near the southern tip of Sri Lanka while freshest waters (< 31 pss) hug the vicinity of the Ganges-Brahmaputra estuary. Following the summer monsoon withdrawal (Figure 7*b*), these northernmost waters further freshen below 30 pss and expand along both western and eastern boundaries. Finally, the eastern and western freshwater tongues gradually erode during winter and spring (Figure 7*c*,*d*). SMOS and

Aquarius data qualitatively capture this basin-scale seasonal evolution (Figure 7*e* to 7*l*). However, some differences between satellite and in situ climatologies can be already noticed: SMOS SSS are fresher than NIOA in the WBoB in summer (Figure 7*a,e*) and Aquarius SSS are fresher than NIOA in the NBoB in fall (Figure 7*b,j*). Large differences can also be found for both satellites in the Andaman Sea but the quality of NIOA climatology there is likely to be strongly hampered by the lack of in situ observations in this region.

Figure 8 further provides a quantitative assessment of the SSS seasonal cycle from the satellites retrieval in the three sub-regions considered (NBoB, CBoB and WBoB) by comparing them to their collocated in situ dataset. First of all, the seasonal evolution of SSS in the three selected boxes from the collocated in situ datasets (black lines on Figure 8) agrees reasonably well with the one derived from the NIOA box average (blue lines on Figure 8), with correlation larger than 0.8. This suggests that the in situ dataset captures the main features of the climatological seasonal cycle depicted by the NIOA dataset despite the limited number of years (around three) and the rather heterogeneous spatial coverage of this in situ dataset (Figure 2*c*,*d*),

In the northern part of the Bay, a 1.5 pss freshening is observed between July and October (black line on Figure 8*a*,*b*) in response to the huge fresh water flux from monsoonal rainfall and Ganges-Brahmaputra river discharge. This freshening is followed by a gradual saltening from November onward. The observed freshening is larger for the in situ dataset collocated with Aquarius (Figure 8*b*) than for the one of SMOS (Figure 8*a*) due to the extended Aquarius data coverage in the northeasternmost part of the Bay (Figure 2*a*,*b*) where the lowest salinities are found. Both satellite retrievals are able to capture this strong seasonal freshening reasonably well but overestimate the freshening signal during the post-monsoon season (red and black lines on Figure 8*a*,*b*). The phase agreement of Aquarius with the in situ dataset is however better than the one derived from SMOS, with correlations of 0.95 and 0.81 respectively.

The WBoB SSS also displays a seasonal freshening similar to that of NBoB but occurring with a two month delay (Figure 8*c*,*d*), corresponding to the time it takes for the fresh waters in the Northern Bay to be advected southward by the East India Coastal Current along the western boundary (Chaitanya *et al.* 2014a, Benshila *et al.* 2014, Akhil *et al.* 2014). The observed freshening in WBoB is also larger for the in situ dataset collocated with Aquarius (Figure 8*d*) than for the one of SMOS (Figure 8*c*). While Aquarius reproduces the seasonal timing of this coastal freshening very accurately (0.9 correlation), SMOS displays a too early seasonal freshening starting in June, with several spurious peaks, resulting in a poor phasing with in situ observations (0.27 correlation).

Finally, the SSS seasonal cycle in CBoB exhibits a semi-annual signal with two salinity minima occurring during fall and spring (Figure 8*e*,*f*). As for WBoB, Aquarius captures very accurately these seasonal variations (0.92 correlation; Figure 8*f*) while SMOS displays an erratic behaviour and is unable to retrieve this seasonal evolution (0.25 correlation; Figure 8*e*).

This validation shows that Aquarius reproduces the observed SSS seasonal cycle well in both near-coastal and open-ocean regions. In contrast, SMOS is unable to capture the seasonal variability south of 16°N, neither in the coastal region along the west coast of India nor in the central part of the Bay.

5. Evaluation of SSS year-to-year variations

As existing in situ climatologies such as NIOA already provide a reasonable description of SSS seasonal variations, a considerable added value of satellite products is their potential to describe SSS departures from the mean seasonal cycle. In order to qualitatively assess the satellites skill in capturing non-seasonal SSS anomalies, Figure 9 displays a scatterplot of each satellite SSS estimates deviations from the NIOA climatology against those from the in situ reference product. A good agreement between satellite estimates and in situ data seasonal anomalies would result in a cloud of points aligned along the $x = y$ axis while a strong underestimation of the non-seasonal variability of the satellite SSS estimates would result in a cloud of points aligned along the $y = 0$ axis. Figure 9*a* and 9*c* reveal that SMOS retrieval considerably underestimates the observed non-seasonal variations and exhibits a poor phase agreement with in situ observations for both pixel-wise and box-averaged comparisons (0.36 and 0.29 correlation, respectively). In contrast with SMOS, Aquarius reasonably captures the amplitude and phase of the observed SSS seasonal anomalies (0.57 and 0.73 correlation for pixel-wise and box-averaged comparison respectively, Figure 9*b*,*d*) and may therefore provide additional valuable information with respect to the information already contained in the existing climatologies.

A more detailed analysis on the ability of the satellites retrieval to capture the temporal evolution in the three boxes where in situ data are available (NBoB, WBoB, CBoB) is further provided on Figure 10. The largest departures from the seasonal climatology occur in the NBoB box, with in situ anomalies ranging between -1.5 and 1.5 pss (Figure 10*a*,*d*). The in situ dataset indicates a freshening anomaly following the 2011 monsoon that lasts until spring 2012, followed by a salty anomaly in the 2012 post-monsoon and 2013 monsoon. Aquarius displays a reasonably good phase agreement with the in situ anomalies in this region (0.75 correlation; Figure 10*d*). In particular, it captures the timing of the anomalous freshening from late 2011 to mid-2012 accurately, although its amplitude is twice larger than in observations in late 2011. Aquarius also captures the anomalous saltening observed during the 2013 monsoon. In contrast, SMOS exhibits a poor phase agreement with in situ anomalies there

(0.33 correlation; Figure 10*a*), being unable to capture neither the early 2012 anomalous freshening nor the mid-2013 saltening.

The WBoB SSS also displays large departures from its climatology, ranging from -1 to 1 pss. For instance, the freshening along the east Indian coastline following the monsoon is stronger than normal in 2010 and weaker than normal in 2011 and 2012 (Figure 10*b*,*e*). Once again, SMOS behaves poorly in this region (0.31 correlation; Figure 10*b*): it does not reproduce well the fresh event in late 2011 and salty events in late 2012 and 2013, only performing well in late 2013. In contrast, Aquarius SSS estimates display a good phase agreement with the in situ dataset over most of the period (0.74 correlation): it is able to capture the abrupt change from salty to fresh anomalies in late 2011, freshening over 2013 and salty anomalies in early 2014. It however misses completely the strong saltening signal evident in the in situ dataset in late 2012.

In CBoB, the departures from the seasonal cycle are weaker than in the NBoB and WBoB boxes, with anomalies that do not exceed 0.5 pss. The in situ SSS displays fresher than normal conditions in early 2012 and most of 2013 and saltier than normal conditions in late 2012. As for the two other boxes, Aquarius accurately captures these departures from the seasonal cycle (0.77 correlation) while SMOS completely fails (0.02 correlation).

As discussed in the previous section, strong departures from the seasonal climatology occur in late 2011 and early 2012 in each of the sub-regions: an anomalous freshening in NBoB from fall 2011 to summer 2012, an anomalous saltening in fall 2011 in WBoB, and an anomalous freshening in spring 2012 followed by a saltening signal in summer 2012 in CBoB. The performance of the two satellites in reproducing the spatial patterns related to these seasonal departures from the climatology is illustrated on Figure 11. The in situ product indeed indicates that the northeastern BoB is fresher than normal in fall 2011, while salty anomalies are observed to the south of 16°N and to the west of 88°E (Figure 11*a*). The freshening in NBoB expands southward along the east coast of India in winter 2012 (Figure 11*b*) and in the central part of the Bay around (15°N; 90°E) in spring 2012 (Figure 11*c*). These anomalies in CBoB reverse sign in summer 2012 (Figure 11*d*), with two cores of salty anomaly observed around (16°N; 86°E) and (10°N; 88°E). Aquarius is able to capture the broad spatial structure of the anomalies depicted by the in situ dataset (Figure 11*e*,*h*). In contrast, although SMOS captures the NBoB freshening in fall 2011 and winter 2012 (Figure 11*i*,*j*), it is unable to capture either the saltening along the eastern coast of India in fall 2011, or the amplitude and spatial extend of the freshening in the CBoB in spring 2012 (Figure 11*k*), or the salty anomalies in summer 2012 (Figure 11*l*). This example thus illustrates the ability of Aquarius to retrieve regional features in the salinity field within the BoB and the caveats related to SMOS retrieval.

6. Summary and discussion

6.1. Summary

The BoB exhibits strong meridional and vertical salinity gradients, with very fresh surface waters to the North. The monitoring of SSS variability there is not straightforward due to insufficient in situ data coverage. This monitoring may benefit from the recent availability of SSS remotely-sensed data. The retrieval of satellite-derived SSS measurements is however very challenging in this region, because the semi-enclosed nature of the BoB may potentially contaminate the SSS signals through radio frequency interferences and land effects. The goal of this study is therefore to perform a validation of the SMOS CEC-IFREMER V02 level-3 1°×1° and Aquarius CAP-V03 level-3 1°×1° gridded monthly salinity retrievals against a comprehensive gridded in situ SSS product in the BoB to infer whether these satellite datasets can confidently be used to describe SSS variations in this climatically important region. We first estimate that our in situ dataset is reasonably representative of 1° × 1° monthly SSS estimates. The instrumental error is negligible (approximately 0.01 pss). The fact that most in situ data are representative of the 5 – 10 m depth layer induces a salty bias of up to 0.06 pss and a RMSE of up to 0.2 pss on the surface salinity estimate. The main source of error is the representation error, i.e. the fact that monthly 1° × 1° SSS estimates are evaluated from a median number of 2 observations per cell, resulting in an estimated RMSE of about 0.3 pss. Collectively, those errors (approximately 0.32 pss RMSE if considered independent) are smaller than the variability in the Bay of Bengal and smaller than the estimated RMSE on individual monthly pixels (around 0.7 pss to 0.9 pss) from both satellites.

Our results reveal large differences in the ability of the SMOS and Aquarius satellite products to retrieve SSS variability. The spatial coverage of the SMOS product is poorer compared to Aquarius, especially in the Northern portion of the BoB. SMOS exhibits a systematic fresh bias everywhere in the Bay of Bengal (-0.19/-0.35 pss depending on the region). In contrast, the mean SSS field retrieved from Aquarius is accurate, except in the northern part of the Bay where it exhibits a -0.26 pss fresh bias. The seasonal variability depicted by Aquarius retrievals is also accurate in the northern, central and western part of the basin with correlations to the reference in situ dataset exceeding 0.9. In contrast, SMOS retrievals fail to represent the SSS seasonal cycle in the western and central part of the basin. Aquarius retrievals are also able to capture departures from the mean seasonal cycle, with a correlation around 0.75 with large-scale year-to-year SSS variations from the in situ dataset in all regions. Aquarius for instance successfully captures the main spatio-temporal features of the anomalous freshening event that occurred in the northern and central part of the BoB in late 2011 and early 2012. In contrast, SMOS estimate generally fails to capture the timing and spatial patterns of SSS departures from the seasonal cycle.

Figure 12 provides a compelling summary of the added value provided by the two satellite retrievals compared to the existing climatologies. The SMOS retrieval indeed displays a poorer phase agreement with the in situ dataset than the NIOA climatology over the WBoB and SBoB and a similar agreement over the NBoB (Figure 12*a*). In contrast, the situation is far more promising for Aquarius, which exhibits higher correlations with in situ observations than SMOS and NIOA over all the sub-regions (Figure 12*b*). This indicates that the current version of Aquarius retrievals provide additional information with respect to the existing SSS climatologies in the BoB, while the version of SMOS SSS assessed here does not.

6.2. Discussion

Preliminary assessments of one-year data from earlier versions of both level-3 SMOS (Subrahmanyam *et al.* 2013, Ratheesh *et al.* 2013) and Aquarius datasets (Ratheesh *et al.* 2014) over the BoB reported major issues in the satellites ability to retrieve SSS there. In this paper, we provide in-depth validations of a more recent version of these level-3 products over a longer period (around 3 years). Our results indicate that the CAP-V03 level-3 1°×1° gridded monthly Aquarius SSS retrieval performs considerably better than earlier versions, especially for low SSS values in the northern part of the Bay. This better performance could be related to an improved roughness correction in this Aquarius product (Yueh *et al.* 2014). In contrast, the CEC-IFREMER V02 level-3 1°×1° SMOS retrieval tested here exhibits significant caveats at both seasonal and non-seasonal timescales. This may be partly related to the relaxation to the climatology used in this version of SMOS. Hernandez *et al.* (2014) actually found better performances for the ESA Level 2 retrieval than for this version in the northern subtropical

Atlantic. As already stated, we however cannot use the ESA level 2 processing because it flags out almost all measurements in the BoB.

Subrahmanyam *et al.* (2013) and Durand *et al.* (2013) reported errors of the order of 0.2 pss for SMOS level-3 data in the southern equatorial Indian Ocean. This indicates that the bad performance of SMOS reported in this paper is specific to the BoB. There can be several reasons behind the contrasted ability of SMOS and Aquarius to capture SSS in the BoB. First, the interferometric nature of SMOS instrument makes its measurements much more sensitive to RFIs than a classical radiometer like Aquarius. Second, SMOS is affected by systematic biases extending to about 1000 km from continents which is until now imperfectly taken into account. Further work is needed to infer if the performance of the SMOS product in the BoB can be improved by updating its algorithm retrieval or of if its performance will anyway be strongly limited by the design of the instruments for this specific region.

Another concern of the present study may be related to fine spatio-temporal scales in the SSS field, which have been spotted in the past in the BoB (e.g. Shetye *et al.* 1996, Hareesh Kumar *et al.* 2013, Chaitanya *et al.* 2014a). This strong spatio-temporal variability raises the question of the representativeness of a couple of individual in situ measurements, against the retrieved SSS from satellite, representative of a larger spatial scale (typically 1°×1°×1 month). The instrumental error is very small (0.01 pss). We did estimate sampling error by taking advantage of the intensive measurements performed at RAMA moorings. The error associated with vertical sampling is generally less than 0.2 pss. The representation error of our in situ reference dataset for monthly 1° × 1° estimates is generally less than 0.3 pss. If those errors are assumed to be independent, the overall RMSE of our in situ dataset is approximately 0.36 pss. This is far from negligible, but generally smaller than the satellite biases discussed in the present study. In addition, the validation of time series average over larger boxes in typical regions of variability (NBOB, WBoB, CBoB) acts to further reduce this representation issue. The smallest of the 3 boxes (WBoB) indeed contains up to 40 individual 1° × 1° × 1 month estimates. Even if our reference in situ product provides SSS estimates for only one half of the grid cells (20 measurements), this results in a box-average RMSE inferior to 0.1 pss (when assuming independent errors). While the error statistics of individual satellite data on the 1°×1°×1 month grid should be taken cautiously (i.e. the RMSE is probably enhanced by the representation error), we thus believe that the error statistics for the entire NBoB, WBoB and CBoB boxes provide a more reasonable evaluation of the actual performance of those satellite products. Another caveat is of course the length of the time series (around 3 years). A more in-depth assessment of the capability of the satellites to estimate the seasonal cycle in the BoB will probably be needed a couple of years down the line, but we believe that the current analysis still clearly points out that, while the current Aquarius large-scale SSS retrieval can be used within the BoB, there is still work to be done to improve existing SMOS retrievals.

6.3. Perspectives

One key-advantage of spaceborne SSS products is their ability to sample regions that are completely devoid of in situ observations. One such region is the Andaman Sea. This region exhibits a large SSS variability in the spaceborne measurements (Figure 2*e*,*f*) and model simulations (Akhil *et al.* 2014). Like the northern part of the Bay, the Andaman Sea is characterized by intense monsoonal rains (Hoyos and Webster 2007) and continental runoff (Furuichi *et al.* 2009). Although no in situ SSS observations are available in this region for the recent period, satellites reveal vigorous signals there (Figure 13). Both SMOS and Aquarius indicate a strong seasonal freshening of about 2 pss during the monsoon and post-monsoon seasons, followed by a subsequent saltening in winter-spring. The magnitude of these SSS changes is comparable to those observed in the northern or western part of the BoB (Figure

8). The Andaman Sea post-monsoon freshening depicted by the two satellites is larger than the one suggested by the NIOA climatology. Due to the very limited availability of salinity data in the Andaman sea (Antonov *et al.* 2010, Chatterjee *et al.* 2012), and relatively good performance of Aquarius in other regions, one is tempted to believe that it is the NIOA climatology that is erroneous here, and that Aquarius brings us an improved knowledge of the seasonal cycle of SSS in the Andaman Sea. Beyond this seasonal picture, both SMOS and Aquarius data suggest a larger seasonal fresh anomaly during and after the 2012 monsoon than during other years. It would be interesting to assess the quality of the spaceborne SSS products in the Andaman Sea, in order to judge if they can be used for monitoring SSS and understand mechanisms of SSS variability there.

It would also be very interesting to better understand the mechanisms driving the interannual SSS variability in the BoB. Using a similar in situ SSS dataset to the one used in this study combined with satellite estimates of rainfall and Ganges-Brahmaputra river runoffs, Chaitanya *et al.* (2014b) already suggested that interannual SSS variability in the northeastern part of the Bay over the 2009-2012 period was primarily driven by freshwater flux variability, and in particular river runoffs. Given the ability of Aquarius to capture the interannual SSS variations in the BoB to a reasonable extent, it is very tempting to perform a similar salt budget to the one of Chaitanya *et al*. (2014b) but using the more spatially complete Aquarius SSS retrieval. Interannual river runoffs data derived from satellite measurements are however only currently available until the end of 2012 (i.e. only 15 months of common data with remotely-sensed SSS) (Papa *et al.* 2012), so far precluding a meaningful investigation of the interannual mixed-layer salt budget in the BoB. Once interannual runoffs data from the main BoB rivers (i.e. Ganges-Brahmaputra and Irrawaddy) become available for the recent years, a promising follow-up of this work would therefore be to use the Aquarius SSS dataset to assess the main processes that control the interannual SSS variations in the various regions of the BoB.

The present study is dedicated to SMOS and Aquarius salinity assessment. Beyond these two pioneering missions, some evolutions in the field of ocean salinity remote sensing are expected shortly. The next generation of spaceborne sensors usable for SSS monitoring, beginning with Soil Moisture Active and Passive (SMAP) satellite (sucessfully launched in January 2015, see smap.jpl.nasa.gov), promises significant progresses in our ability to retrieve valuable spaceborne estimates of SSS field in the global ocean. We believe our study, focused on one of the most challenging areas of the world ocean, paves the way for the future of spaceborne salinity science there.

Acknowledgements

This study is supported by the LEFE/EC2CO project GEOMOD (AO2015- 873251) from the French National Institute of Sciences of the Universe (CNRS / INSU). We also acknowledge the financial support by a TOSCA project from CNES, the French Space Agency. AVP was funded through a PhD grant from CNES and IRD. We thank IRD for the financial support for the Indo-French collaboration on Indian Ocean research. In situ SSS samples are collected under support from Ministry of Earth Sciences (Government of India). We are thankful to the numerous people involved in the ARGO and RAMA projects. We sincerely thank the team efforts of technical and scientific staff from National Institute of Ocean Technology, Chennai, India for providing continuous data from the OMNI moorings. Thermosalinograph data were collected and processed by the French SSS Observation Service (www.legos.obs-mip.fr/observations/sss). CNES partly funded these activities in the frame of the CATDS and of the SMOS TOSCA projects. We acknowledge constructive discussions with Nicolas Reul. We also thank him for sharing the CATDS SMOS level-3 datasets. Clement de Boyer Montegut is supported by the European Union via the seventh Framework Programme (INCO_LAB) GA295092 (INDO-MARECLIM).

References

Akhil, V.P., Durand, F., Lengaigne, M., Vialard, J., Keerthi, M. G., Gopalakrishna, V.V., Deltel, C., Papa, F. and de Boyer Montégut,C., 2014, A modeling study of the processes of surface salinity seasonal cycle in the Bay of Bengal. *J. Geophys. Res.*, 116, 3926-3947, doi : 10.1002/2013JC009632

Alory G., Delcroix, T., Téchiné, P., Diverrès, D., Varillon, D., Cravatte, S., Gouriou, Y., Grelet, J., Jacquin, S., Kestenare, E., Maes, C., Morrow, R., Perrier, J., Reverdin, G., Roubaud, F., 2015, The French contribution to the Voluntary Observing Ships network of Sea Surface Salinity. *Deep Sea Research*, in press.

Antonov, J. I., Seidov, D., Boyer,T.P., Locarnini, R. A., Mishonov, A.V., Garcia, H. E., Baranova, O. K., Zweng, M.M. and Johnson,D.R., 2010, World Ocean Atlas 2009. *Volume 2: Salinity. S. Levitus, Ed. NOAA Atlas NESDIS 69*, U.S. Government Printing Office, Washington, D.C., 184 pp.

Benshila, R., Durand, F., Masson S., Bourdalle-Badie, R., de Boyer Montégut, C., Papa, F. and Madec, G., 2014, The upper Bay of Bengal salinity structure in a high-resolution model. *Ocean Modelling*, 74, 36-52.

Boutin, J., Martin, N., Yin, X., Font, J., Reul, N. and Spurgeon, P., 2012, First assessment of SMOS data over open ocean: part II Sea Surface Salinity. *IEEE Transactions on Geoscience and Remote Sensing*, doi: 10.1109/TGRS.2012.2184546.

Chaitanya, V.S., Lengaigne, M., Vialard, J., Gopalakrishna, V. V., Durand, F., KranthiKumar, C., Amrithash, S., Suneel, V., Papa, F. and Ravichandran, M., 2014a, Fishermen-operated salinity measurements reveal a "river in the sea" flowing along the east coast of India. *BAMS*, doi:http://dx.doi.org/10.1175/BAMS-D-12-00243.1

Chaitanya AVS., Durand, F., Mathew, S., Gopalakrishna, V.V., Papa, F., Lengaigne, M., Vialard, J., Krantikumar, C. and Venkatesan, R., 2014b, Observed year-to-year sea surface salinity variability in the Bay of Bengal during the period 2009-2014. *Ocean Dynamics*, doi:10.1007/s10236-014-0802-x.

Chakraborty, A., R. Sharma, R. Kumar, and S. Basu (2014), A SEEK filter assimilation of sea surface salinity from Aquarius in an OGCM: Implication for surface dynamics and thermohaline structure, J. Geophys. Res. Oceans, 119, 4777–4796, doi:10.1002/ 2014JC009984.

Chatterjee, A., Shankar, D., Shenoi, S.S.C., Reddy, G.V., Michael, G.S., Ravichandran, M., Gopalkrishna, V.V., Rama Rao, E. P., Udaya Bhaskar, T.V.S. and Sanjeevan, V.N., 2012, A new atlas of temperature and salinity for the north Indian Ocean, *J. Earth Syst. Sci*., 121(3), 559–593, doi:10.1007/s12040-012-0191-9.

Durand, F., Alory, G., Dussin, R. and Reul, N., 2013, SMOS reveals the signature of Indian Ocean Dipole events. *Ocean Dynamics.*,63(11-12):1203-1212, doi:10.1007/s10236-013-0660-y

Furuichi, T., Win, Z. and Wasson, R.J., 2009, Discharge and suspended sediment transport in the Ayeyarwady River, Myanmar: centennial and decadal changes. *Hydrol. Process*, 23, 1631–1641.doi: 10.1002/hyp.7295

Gierach, M. M., Vazquez-Cuervo, J., Lee, T. and Tsontos, V.M., 2013, Aquarius and SMOS detect effects of an extreme Mississippi River flooding event in the Gulf of Mexico. *Geophys. Res. Lett*., 40, 5188–5193, doi:10.1002/grl.50995.

Hareesh Kumar, P. V., Matthew, B., Ramesh Kumar, M. R., Rao, A.R., Jagadesh, P.S.V., Radhakrishnan, K. G. and Shyni, T.N., 2013, ‘Thermohaline front’ off the east coast of India and its generating mechanism. *Oc. Dyn.,* doi: 10.1007/s10236-013-0652-y

Hasson, A., Delcroix, T., Boutin, J., Dussin, R. and Ballabrera-Poy, J., 2014, Analyzing the 2010–2011 La Niña signature in the tropical Pacific sea surface salinity using in situ data, SMOS observations, and a numerical simulation. *Journal of Geophysical Research: Oceans,* 119, 3855–3867, doi*:*10.1002/2013JC009388.

Hernandez, O., Boutin, J., Kolodziejczyk, N., Reverdin, G., Martin, N., Gaillard, F., Reul, N. and Vergely, J.L., 2014, SMOS salinity in the subtropical north Atlantic salinity maximum: 1. Comparison with Aquarius and in situ salinity. *J. Geophys. Res.*, doi: 10.002/2013JC009610

Hoyos, C.D. and Webster, P.J., 2007, The role of intraseasonal variability in the nature of Asian monsoon precipitation. *J. Clim*., 20, 4402–4424.

Kerr, Y. H., et al., 2010, The SMOS Mission: New Tool for Monitoring Key Elements of the Global Water Cycle. *Proceedings of the IEEE, 98*(5), 666-687.

Lagerloef, G., et al., 2008, The Aquarius/SAC-D mission: Designed to meet the salinity remote sensing challenge. *Oceanography, 21*(1), 68–81 doi:10.5670/oceanog.2008.68.

Lagerloef, G., et al., 2013, Aquarius data release V2.0 validation analysis, Aquarius Proj. Doc. AQ-014-PS-0016. [Available at ftp://podaac-ftp.jpl.nansa.gov/allData/aquarius/docs/v2/AQ-014-PS-0016_AquariusSalinityDataValidationAnalysis_DatasetVersion2.0.pdf.]

Locarnini, R.A., Mishonov, A.V., Antonov, J.I., Boyer, T.P., Garcia, H.E., Baranova, O.K., Zweng, M.M. and Johnson, D.R., 2010 World Ocean Atlas, 2009. *vol 1. In: Levitus TS (ed) NOAA Atlas NESDIS 68. U.S. Government Printing Office,* Washington, DC.

McMullan, K. D., Brown, M.A., Martin-Neira, M., Rits, W., Ekholm, S., Marti, J. and Lemanczyk, J., 2008, SMOS: The Payload. *IEEE Transactions on Geoscience and Remote Sensing.*, 46(3), 594-605.

Mecklenburg, S., Kerr, Y., Font, J. and Hahne A., 2008, The Soil Moisture and Ocean Salinity (SMOS) Mission - An overview, *Geophysical Research Abstracts*, 10.

Mecklenburg, S., Drusch, M., Kerr, Y.H., Font, J., Martin-Neira, M., Delwart, S., Buenadicha, G., Reul, N., Daganzo-Eusebio, E., Oliva, R. and Crapolicchio, R., 2012, ESA's Soil Moisture and Ocean Salinity Mission: Mission Performance and Operations. *IEEE Transactions on Geoscience and Remote Sensing, 50(5),* Part 1:1354-1366.

McPhaden, M. J., Meyers, G., Ando, K., Masumoto, T., Murty, V.S.N., Ravichandran, M., Syamsudin, F., Vialard, J., Yu, L. and Yu, W., 2009, RAMA: The Research Moored Array for African-Asian-Australian Monsoon Analysis and Prediction. *Bull. Am. Meteorol Soc.*, 90,459-480.

Menezes, V. V., Vianna, M. L. and Phillips, H.E., 2014, Aquarius sea surface salinity in the South Indian Ocean: Revealing annual-period planetary waves. *J. Geophys. Res. : Oceans*, 119, 3883–3908, doi:10.1002/2014JC009935.

Neetu, S., Lengaigne, M., Vincent, E. M., Vialard, J., Madec, G., Samson, G., Ramesh Kumar, M.R. and Durand F., 2012, Influence of upper-ocean stratification on tropical cyclone-induced surface cooling in the Bay of Bengal. *J. Geophys. Res.*, 117, C12020, doi: 10.1029/2012JC008433.

Papa, F., Bala, S.K., Pandey, R.K., Durand, F., Gopalakrishna, V.V., Rahman, A. and Rossow, W.B., 2012, Ganga–Brahmaputra river discharge from Jason-2 radar altimetry: an update to the long-term satellite-derived estimates of continental freshwater forcing flux into the Bay of Bengal. J. Geophys. Res. 117, C11021. http://dx.doi.org/10.1029/2012JC008158.

Rao, R. R. and Sivakumar, R., 2003, Seasonal variability of sea surface salinity and salt budget of the mixed layer of the north Indian Ocean. *J. Geophys. Res.*, 108, 3009. doi: 10.1029/2001JC000907.

Ratheesh, S., Mankad, B., Basu, S., Kumar, R. and Sharma R., 2013, Assessment of Satellite-Derived Sea Surface Salinity in the Indian Ocean. *IEEE Geoscience and Remote Sensing Letters 10(3),* 428-431, doi 10.1109/LGRS.2012.2207943.

Ratheesh, S., Sharma, R., Sikhakolli, R., Kumar, R. and Basu, S., 2014, Assessing Sea Surface Salinity Derived by Aquarius in the Indian Ocean. *IEEE Geoscience and Remote Sensing Letters,* 11(4), 719-722.

Reul, N., Tenerelli, J., Boutin, J., Chapron, B., Paul, F., Brion, E., Gaillard, F. and Archer, O., 2012, Overview of the First SMOS Sea Surface Salinity Products. Part I: Quality Assessment for the Second Half of 2010. *IEEE Transactions on Geoscience and Remote Sensing, 50(5),* Part 1:1636-1647.

Reul, N., Fournier, S., Boutin, J., Hernandez, O., Maes, C., Chapron, B., Alory, G., Quilfen, Y., Tenerelli, J., Morisset, S., Kerr, Y., Mecklenburg, S. and Delwart, S., 2013, Sea Surface Salinity Observations from Space with the SMOS Satellite: A New Means to Monitor the Marine Branch of the Water Cycle. *Surv Geophys.*, doi 10.1007/s10712-013-9244-0.

Reul N., Chapron, B., Lee, T., Donlon, C., Boutin, J. and Alory, G., 2014, Sea surface salinity structure of the meandering Gulf Stream revealed by SMOS sensor. *Geophys. Res.Lett.*, 41, 3141–3148, doi:10.1002/2014GL059215.

Roemmich, D., Johnson, G.C., Riser, S., Davis, R., Gilson, J., Owens, W.B., Garzoli, S.L., Schmid, C., Ignaszewski, M., 2009, The Argo Program: Observing the global ocean with profiling floats. *Oceanography,* 22(2):34–43, doi:10.5670/oceanog.2009.36

Shenoi, S. S. C., Shankar, D. and Shetye, S. R., 2002, Difference in heat budgets of the near-surface Arabian Sea and Bay of Bengal: Implications for the summer monsoon, *J. Geophys. Res.*, 107, 3052, doi: 10.1029/ 2000JC000679.

Shetye, S. R., Gouveia, A. D., Shankar, D., Michael, G.S. and Nampoothiri, G., 1996, Hydrography and circulation of the western Bay of Bengal during the Northeast Monsoon. *J. Geophys. Res.*, 101, 14,011 – 14,025.

Subrahmanyam, B., Grunseich, G. and Nyadjro, E.S., 2013, Preliminary SMOS Salinity Measurements and Validation in the Indian Ocean. *IEEE Trans. on Geosci. and Remote Sens.*, vol 51, no. 1,pp. 19-27, jan. 2013.

Tang, W., Yueh, S. H., Fore, A. G., Hayashi, A., Lee, T. and Lagerloef, G., 2014, Uncertainty of Aquarius sea surface salinity retrieved under rainy conditions and its implication on the water cycle study. *J. Geophys. Res.: Oceans*, *119*(8), 4821-4839.

Terray, L., Corre, L., Cravatte, S., Delcroix, T., Reverdin, G. and Ribes, A., 2012, Near-surface salinity as nature's rain gauge to detect human influence on the tropical water cycle. *J. Clim.*, 25, 958–977, doi:10.1175/JCLI-D-10-05025.1.

Venkatesan, R., Shamji, V. R., Latha, G., Mathew, S., Rao, R. R., Muthiah, A. and Atmanand, M. A., 2013, In situ ocean subsurface time-series measurements from OMNI buoy network in the Bay of Bengal. *Current Science (Bangalore)*, 104(9), 1166-1177.

Vinayachandran, P. N. and Nanjundiah, R.S., 2009, Indian Ocean sea surface salinity variations in a coupled model. *Clim. Dyn.*, doi: 10.1007/s00382–008–0511–6.

Yueh S, Tang, W., Fore, A., Hayashi, A., Song, Y. T. and Lagerloef, G., 2014,Aquarius geophysical model function and combined active passive algorithm for ocean surface salinity and wind retrieval. J. Geophys. Res. Oceans, 119, 5360–5379, doi: 10.1002/2014JC009939.

Zhang, H., Ge Chen., Chengcheng Qian. and Haoyu Jiang., 2013, Assessment of Two SMOS Sea Surface Salinity Level 3 Products Against Argo Upper Salinity Measurements. *Geoscience and Remote Sensing Letters, IEEE*, 10 (6), 1434-1438.

Zweng, M.M., Reagan, J.R., Antonov, J.I., Locarnini, R.A., Mishonov,A.V., Boyer, T.P., Garcia, H. E., Baranova, O.K., Johnson, D.R., Seidov, D. and Biddle, M.M., 2013, World Ocean Atlas 2013. *Volume 2: Salinity. S. Levitus, Ed., A. Mishonov Technical Ed.; NOAA Atlas NESDIS 74*, 39 pp.

Figure Captions:

Figure 1. Climatological Sea Surface Salinity (SSS) in the Bay of Bengal (BoB) from the North Indian Ocean Atlas (NIOA, Chatterjee et al., 2012) for ***(a)*** June-July-August (JJA), ***(b)*** September-October-November (SON), ***(c)*** December-January-February (DJF), and ***(d)*** March-April-May (MAM).

Figure 2. Percentage of valid monthly SSS retrievals in the Bay of Bengal for **(*a*)** SMOS and **(*b*)** Aquarius. Total number of in situ observations profiles per 1°×1° box and per year (No. Obs) collocated with **(*c*)** SMOS and **(*d*)** Aquarius. Circles on panels *c* and *d* indicate RAMA mooring locations, while triangles indicate OMNI moorings. The two continuous lines on panels *c*,*d* indicate merchant ships tracks between Port Blair (PB) and Chennai (C) / Kolkata (K), along which approximately 1200 XCTD and bucket measurements were collected. The dotted line indicates the merchant ship track along which thermosalinograph measurements are performed. **(*e*)** SMOS and **(*f*)** Aquarius SSS standard deviation. The standard deviation on panels *e*,*f* is only shown for pixels with more than 11 months of data. The red boxes on panels (*e*) and (*f*) indicate the limits of the NBoB (86°E-94°E; 16°N-23°N), WBoB (80°E-84°E; 6°N-16°N), CBoB (84°E-94°E; 6°N-16°N) and Andaman Sea (94°E-99°E; 6°N-18°N), for future reference.

Figure 3. Scatterplots of 1 m depth versus 10 m depth daily salinity measurements for the three Bay of Bengal RAMA moorings at **(*a*)** 90°E8°N, **(*b*)** 90°E12°N and **(*c*)** 90°E15°N.

Figure 4. **(*a*)** Mean correlation coefficient and **(*b*)** Root Mean Square Error between monthly average 1m depth salinity at the three BoB RAMA moorings and subsampled estimates of the monthly average using from 1 to 15 observations. The statistics were computed from 1000 random subsampling of the monthly data. This plot provides an estimate of the representation error arising from subsampling in our validation in situ SSS dataset.

Figure 5. Scatter plot of **(*a*)** SMOS and **(*b*)** Aquarius monthly 1° × 1° SSS retrievals against collocated estimates from the gridded in situ dataset. The statistics are computed from May 2010 to December 2013 for SMOS and from August 2011 to June 2014 for Aquarius. The corresponding correlation coefficient (*r*), root-mean square error (RMSE) and bias are

provided on the lower right of each panel. Values in brackets were estimated using only collocated SMOS, Aquarius and in situ data (i.e. the same spatio-temporal sampling is used for both datasets, and the statistics for the two satellites are hence strictly comparable). **(*c*)** and **(*d*)** are similar to (*a*) and (*b*), but for averaged monthly SSS values over the boxes displayed on Figure 2*e, f*. Blue dots indicate collocated data located in NBOB, green in WBOB and red in CBOB, while black triangles indicate collocated data outside these boxes. The black line indicates median value of each 1pss in situ SSS bin while vertical bars indicate the upper and lower quartiles of the distribution.

Figure 6. (*a*) Systematic bias, **(*b*)** correlation coefficient and **(*c*)** RMSE of box averaged satellite SSS retrievals (SMOS in Bright shade and Aquarius in Light shade) against box-averaged gridded in situ SSS dataset over each sub-region of the Bay of Bengal.

Figure 7. (Upper panels) Climatological Sea Surface Salinity (SSS, pss) in the Bay of Bengal (BoB) for **(*a*)** June-July-August (JJA), **(*b*)** September-October-November (SON), **(*c*)** December-January-February (DJF), and **(*d*)** March-April-May (MAM) from NIOA climatology. **(Middle panels)** Same for SMOS climatological seasonal cycle computed over May 2010 - December 2013 period. **(Bottom panels)** Same for Aquarius climatological seasonal cycle computed over August 2011- June 2014 period.

Figure 8. Time series of the SSS climatological seasonal cycle in **(*a*)** NBoB, **(*c*)** WBoB and **(*e*)** CBoB (outlined on Figure 2*e,f*) from the gridded in situ product (black line), collocated SMOS retrieval (red line), and box-averaged NIOA climatology (blue line). **(*b,d,f*)** Same as (*a,c,e*) but for Aquarius retrieval. The correlation coefficient (*r*) value between in situ and satellite estimates is given on each panel.

Figure 9. As in Figure 5 but for SSS anomalies with respect to the mean climatological seasonal cycle from the NIOA climatology.

Figure 10. Time series of box-averaged monthly SSS interannual anomalies over the **(*a*)** NBoB, **(*b*)** WBoB and **(*c*)** CBoB from the gridded in situ product (black line) and SMOS retrieval (red line). **(*d,e,f*)** Same as (*a,b,c*) but for Aquarius (red line). The grey shading indicates seasons for which the maps of Figure 11 are plotted.

Figure 11. Mean SSS interannual anomalies for **(first column)** September to November 2011, **(second column)** December 2011 to February 2012, **(third column)** March to May 2012, **(fourth column)** and June to August 2012 from **(first row)** the gridded in situ dataset, **(second row)** Aquarius and **(third row)** SMOS.

Figure 12. (*a*) Correlation coefficient of SMOS SSS retrieval (coloured bars) and NIOA climatology (coloured frames) against the gridded in situ SSS dataset over each sub-region of the Bay of Bengal. **(*b*)** Same as (*a*) but for Aquarius.

Figure 13. (*a*) Box-averaged monthly time series of SSS from SMOS (red) and NIOA climatology (blue) for the Andaman Sea box (framed on Figure 2*e*,*f*). **(*b*)** Same as (*a*) but for Aquarius (green).

Figure list

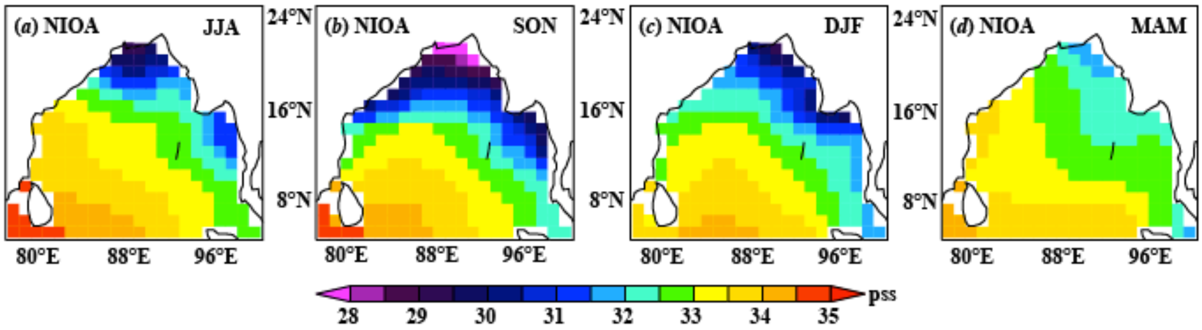

Figure 1

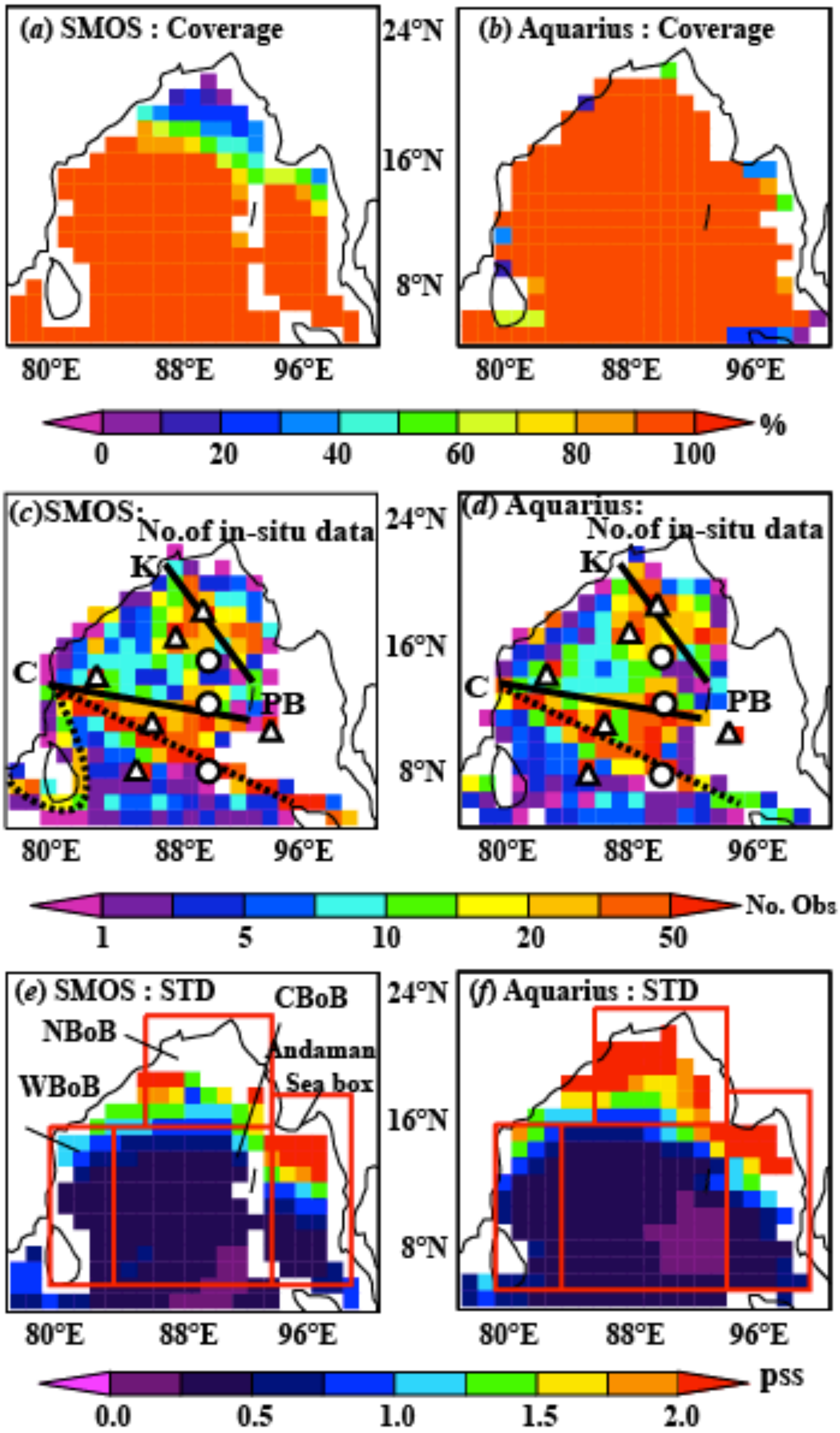

939

940 **Figure 2**

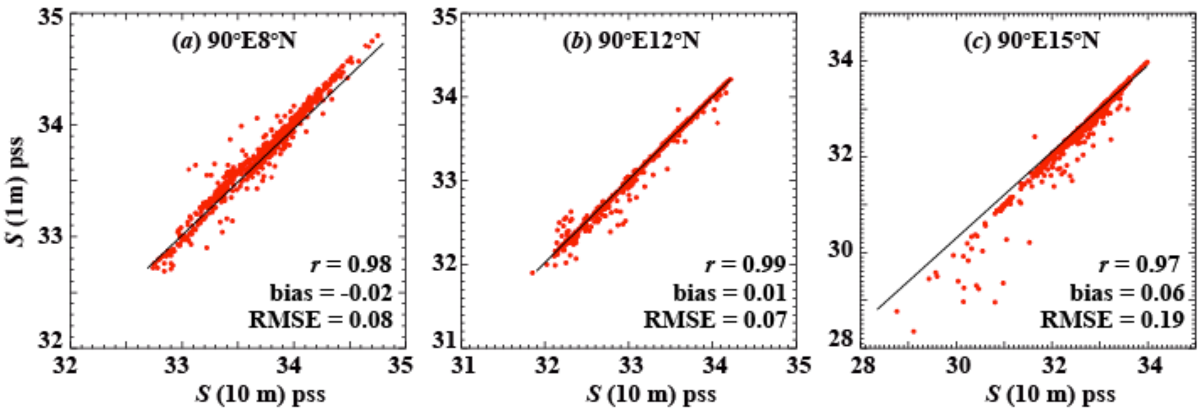
(a) 90°E8°N
r = 0.98
bias = -0.02
RMSE = 0.08
(b) 90°E12°N
r = 0.99
bias = 0.01
RMSE = 0.07
(c) 90°E15°N
r = 0.97
bias = 0.06
RMSE = 0.19
S (1 m) pss
S (10 m) pss
S (10 m) pss
S (10 m) pss

Figure 3

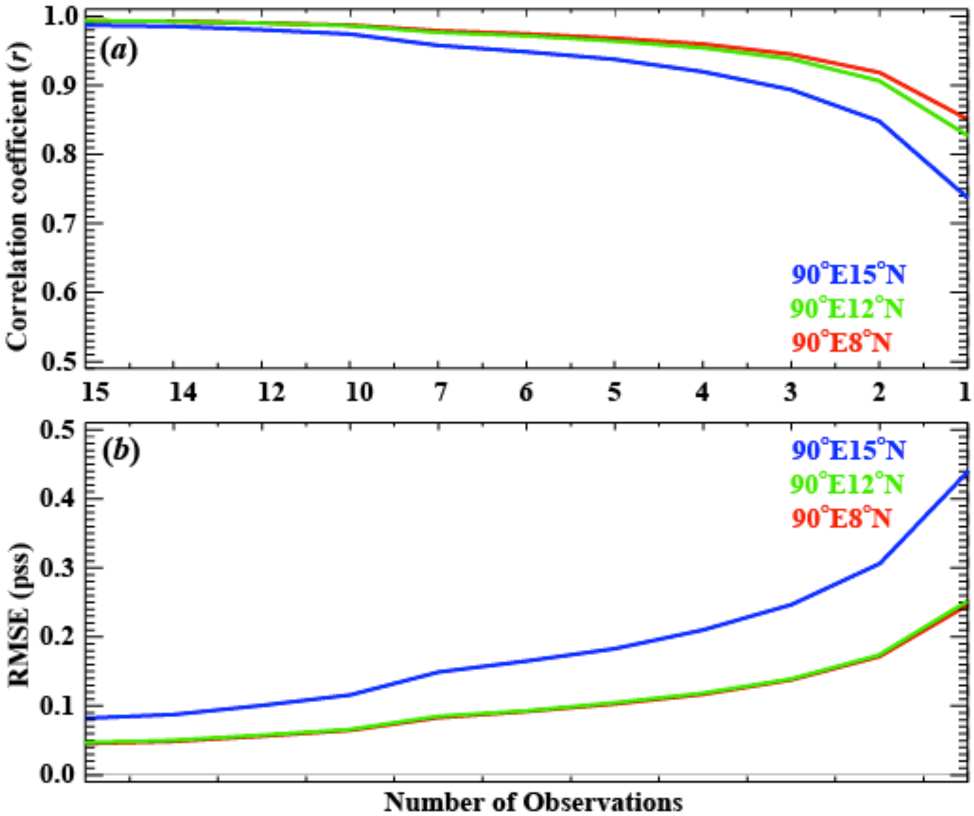

(a)
Correlation coefficient (r)
1.0
0.9
0.8
0.7
0.6
0.5
90°E15°N
90°E12°N
90°E8°N
15
14
12
10
7
6
5
4
3
2
1
(b)
RMSE (pss)
0.5
0.4
0.3
0.2
0.1
0.0
90°E15°N
90°E12°N
90°E8°N
Number of Observations

Figure 4

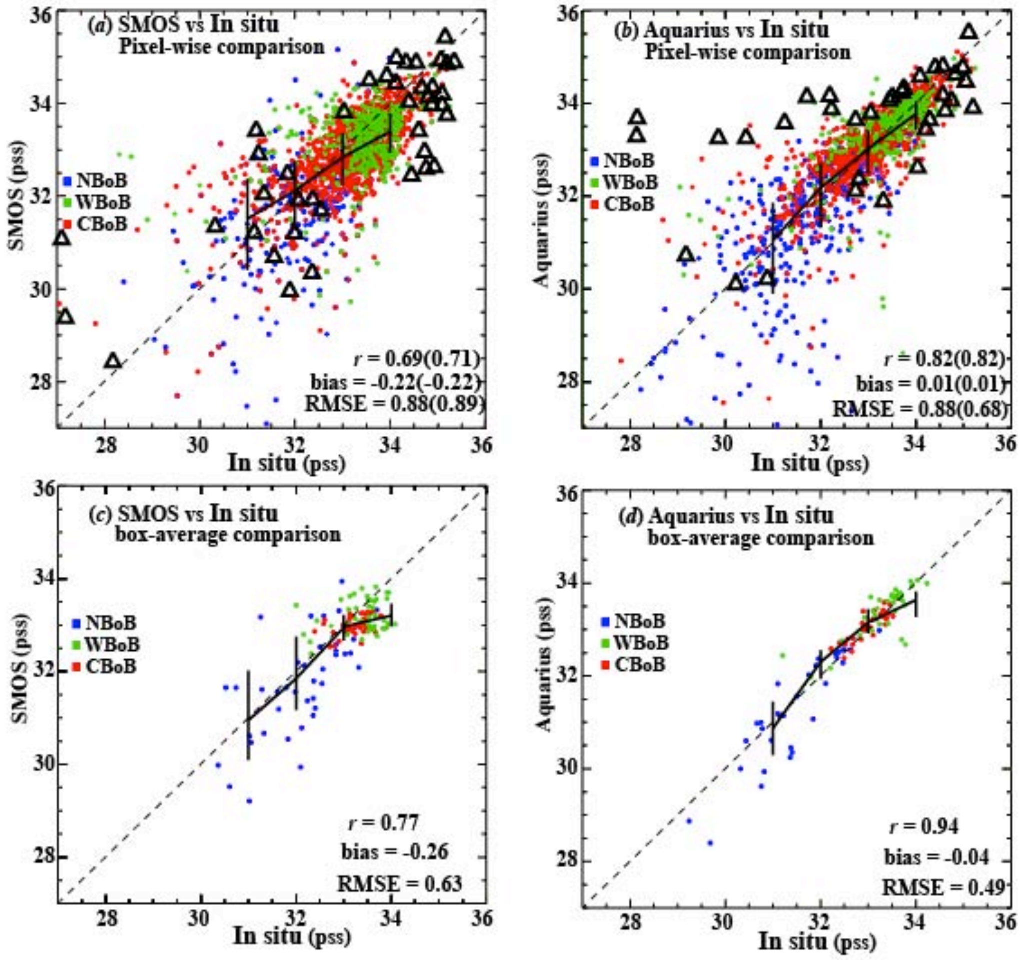
(a) SMOS vs In situ
Pixel-wise comparison
NBoB
WBoB
CBoB
r = 0.69(0.71)
bias = -0.22(-0.22)
RMSE = 0.88(0.89)
SMOS (pss)
In situ (pss)
(b) Aquarius vs In situ
Pixel-wise comparison
r = 0.82(0.82)
bias = 0.01(0.01)
RMSE = 0.88(0.68)
Aquarius (pss)
(c) SMOS vs In situ
box-average comparison
r = 0.77
bias = -0.26
RMSE = 0.63
(d) Aquarius vs In situ
box-average comparison
r = 0.94
bias = -0.04
RMSE = 0.49

Figure 5

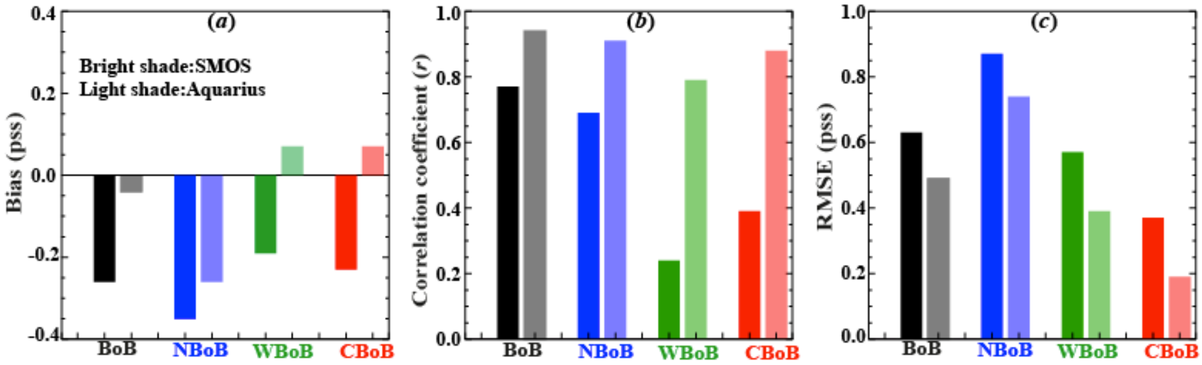
(a)
Bright shade:SMOS
Light shade:Aquarius
Bias (pss)
0.4
0.2
0.0
-0.2
-0.4
BoB
NBoB
WBoB
CBoB
(b)
Correlation coefficient (r)
1.0
0.8
0.6
0.4
0.2
0.0
BoB
NBoB
WBoB
CBoB
(c)
RMSE (pss)
1.0
0.8
0.6
0.4
0.2
0.0
BoB
NBoB
WBoB
CBoB

Figure 6

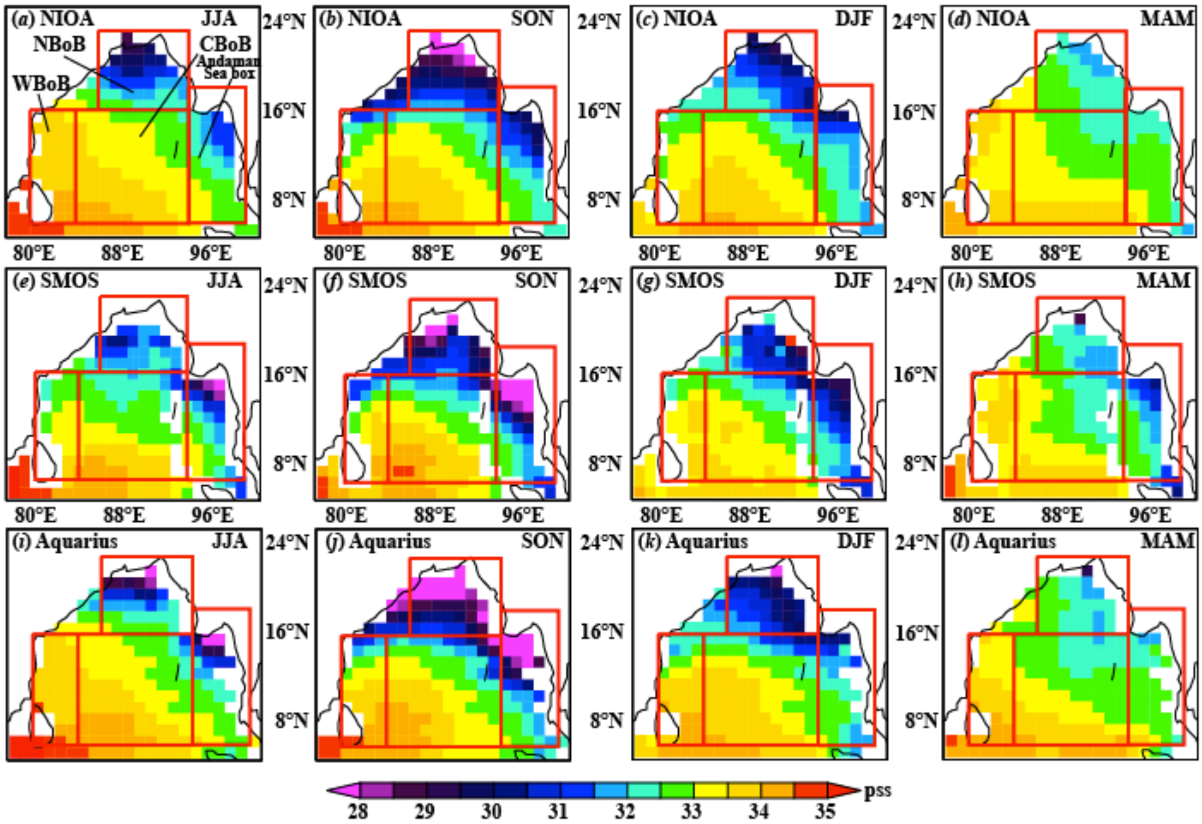

949

950 **Figure 7**

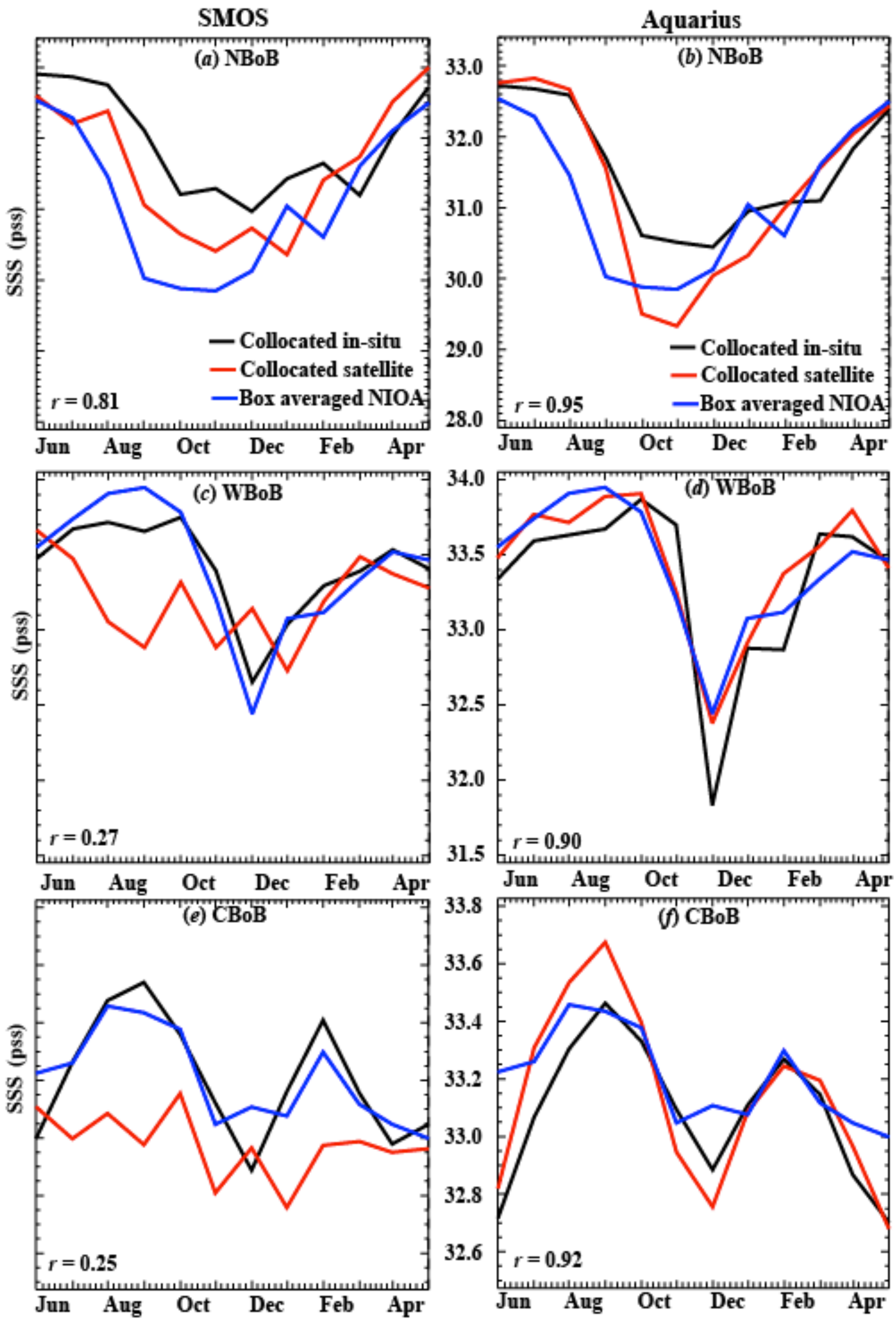
SMOS
Aquarius
(a) NBoB
(b) NBoB
(c) WBoB
(d) WBoB
(e) CBoB
(f) CBoB
SSS (pss)
Collocated in-situ
Collocated satellite
Box averaged NIOA
r = 0.81
r = 0.95
r = 0.27
r = 0.90
r = 0.25
r = 0.92
Jun Aug Oct Dec Feb Apr
33.0 32.0 31.0 30.0 29.0 28.0
34.0 33.5 33.0 32.5 32.0 31.5
33.8 33.6 33.4 33.2 33.0 32.8 32.6

Figure 8

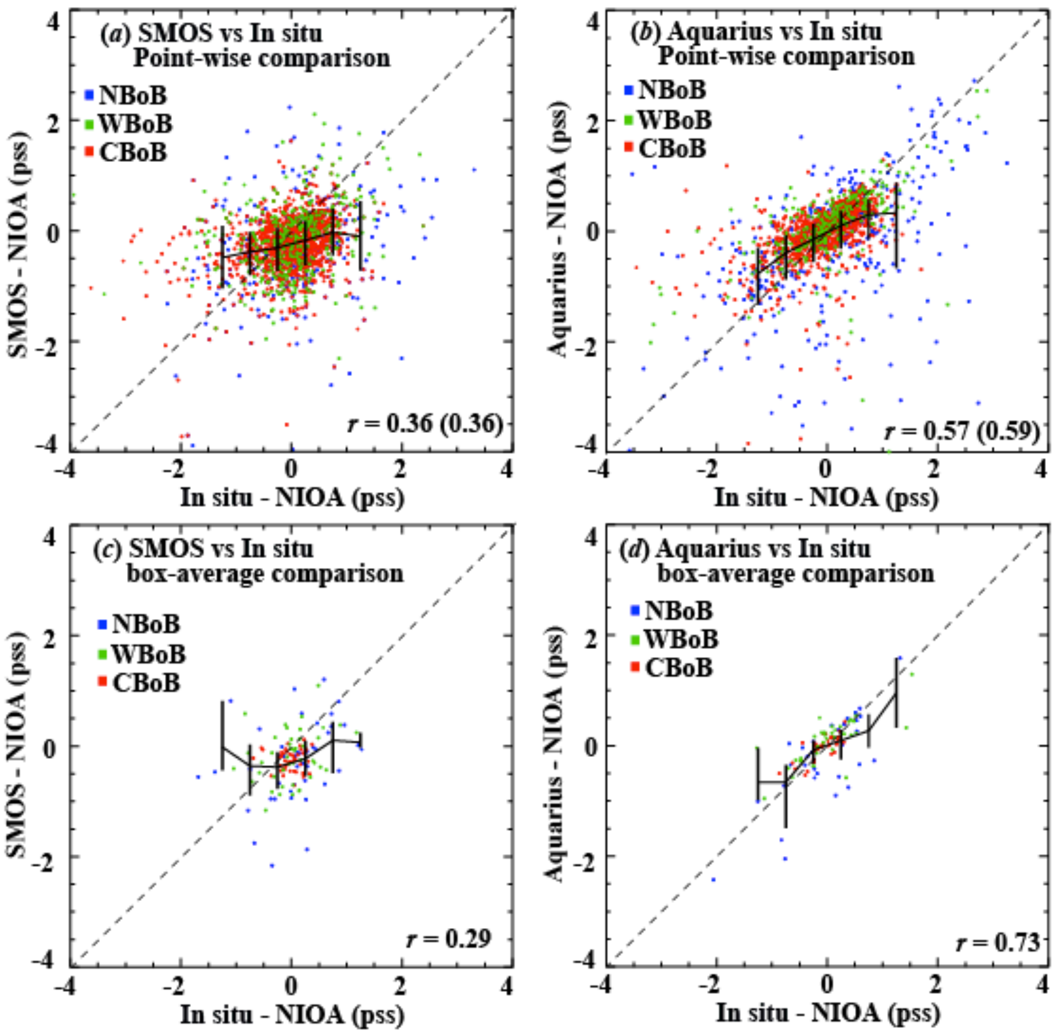
(a) SMOS vs In situ
Point-wise comparison
NBoB
WBoB
CBoB
r = 0.36 (0.36)
SMOS - NIOA (pss)
In situ - NIOA (pss)
(b) Aquarius vs In situ
Point-wise comparison
NBoB
WBoB
CBoB
r = 0.57 (0.59)
Aquarius - NIOA (pss)
In situ - NIOA (pss)
(c) SMOS vs In situ
box-average comparison
NBoB
WBoB
CBoB
r = 0.29
SMOS - NIOA (pss)
In situ - NIOA (pss)
(d) Aquarius vs In situ
box-average comparison
NBoB
WBoB
CBoB
r = 0.73
Aquarius - NIOA (pss)
In situ - NIOA (pss)

Figure 9

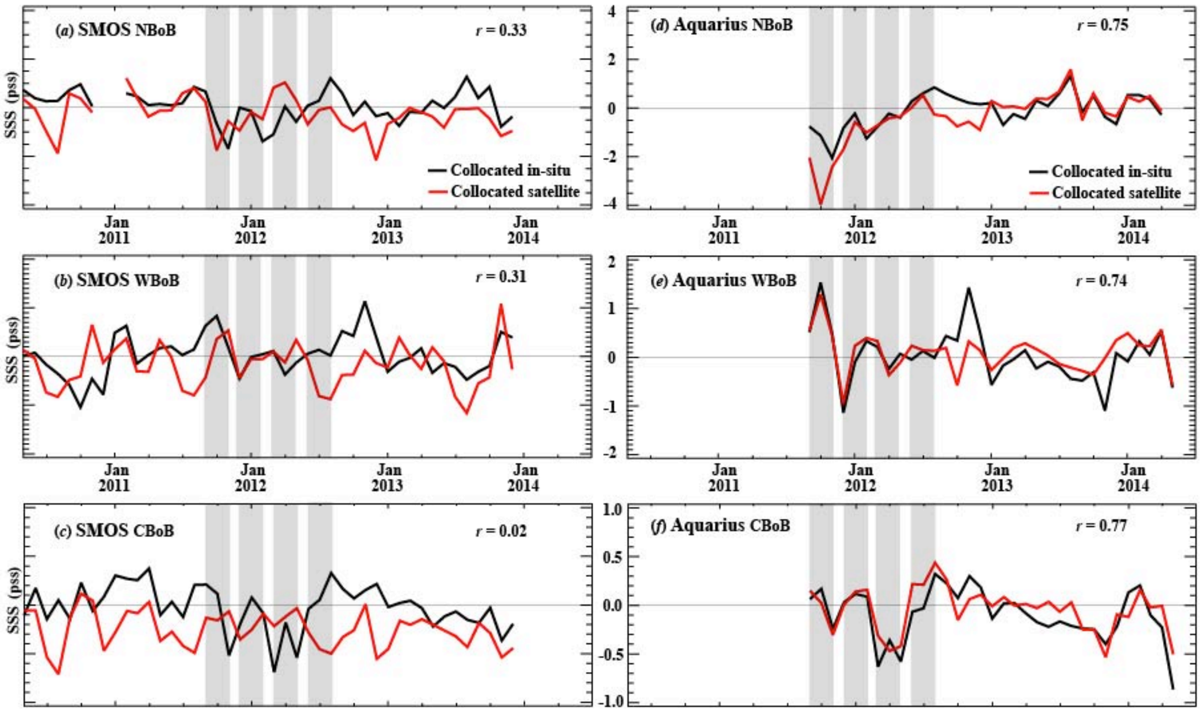
(a) SMOS NBoB
r = 0.33
(b) SMOS WBoB
r = 0.31
(c) SMOS CBoB
r = 0.02
(d) Aquarius NBoB
r = 0.75
(e) Aquarius WBoB
r = 0.74
(f) Aquarius CBoB
r = 0.77
Collocated in-situ
Collocated satellite
SSS (pss)
Jan 2011
Jan 2012
Jan 2013
Jan 2014

Figure 10

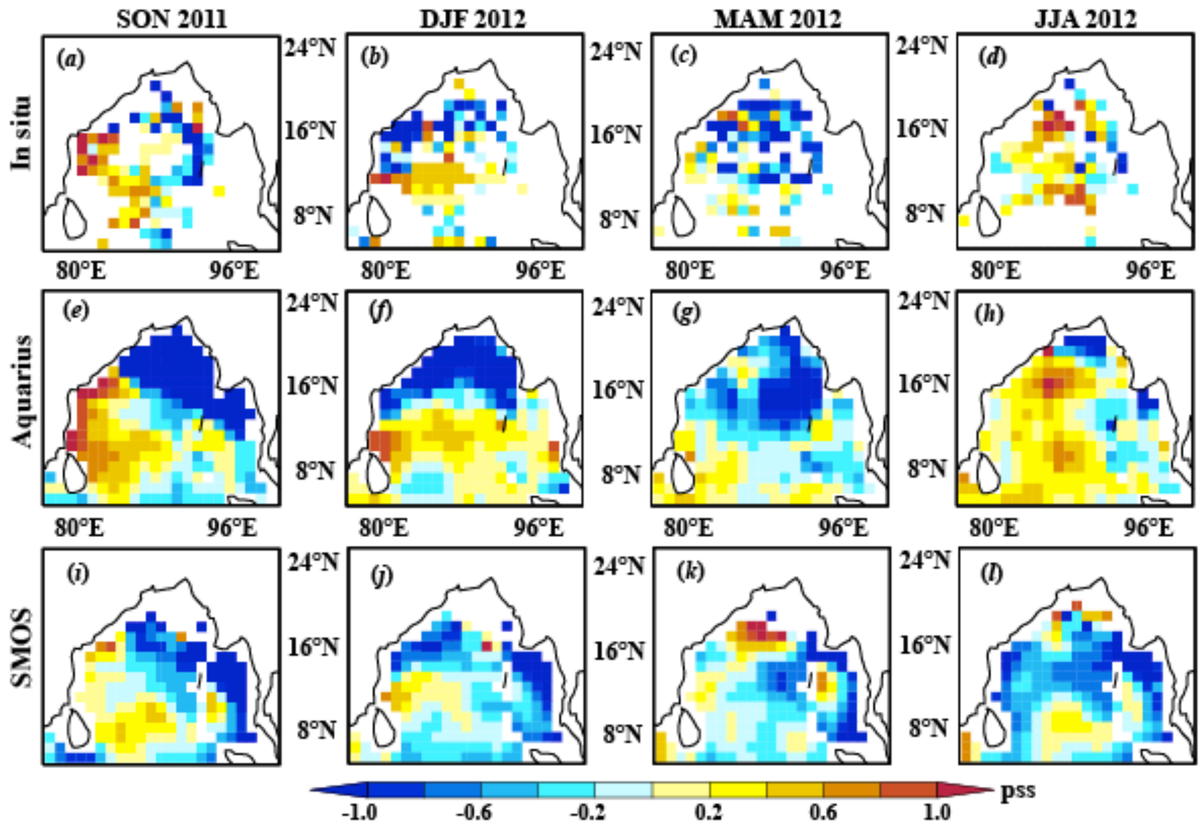

SON 2011
DJF 2012
MAM 2012
JJA 2012
In situ
Aquarius
SMOS
(a)
(b)
(c)
(d)
(e)
(f)
(g)
(h)
(i)
(j)
(k)
(l)
24°N
16°N
8°N
80°E
96°E
-1.0
-0.6
-0.2
0.2
0.6
1.0
pss

Figure 11

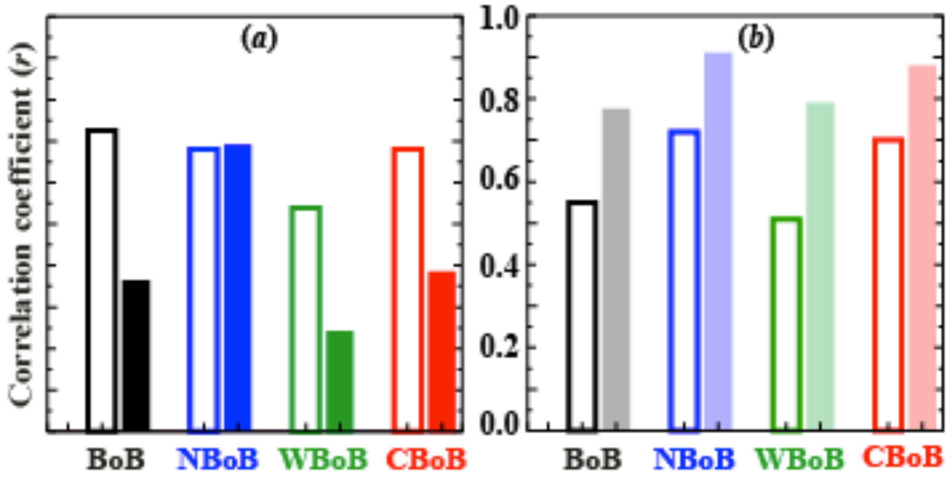
(a)
(b)
Correlation coefficient (r)
1.0
0.8
0.6
0.4
0.2
0.0
BoB
NBoB
WBoB
CBoB
BoB
NBoB
WBoB
CBoB

Figure 12

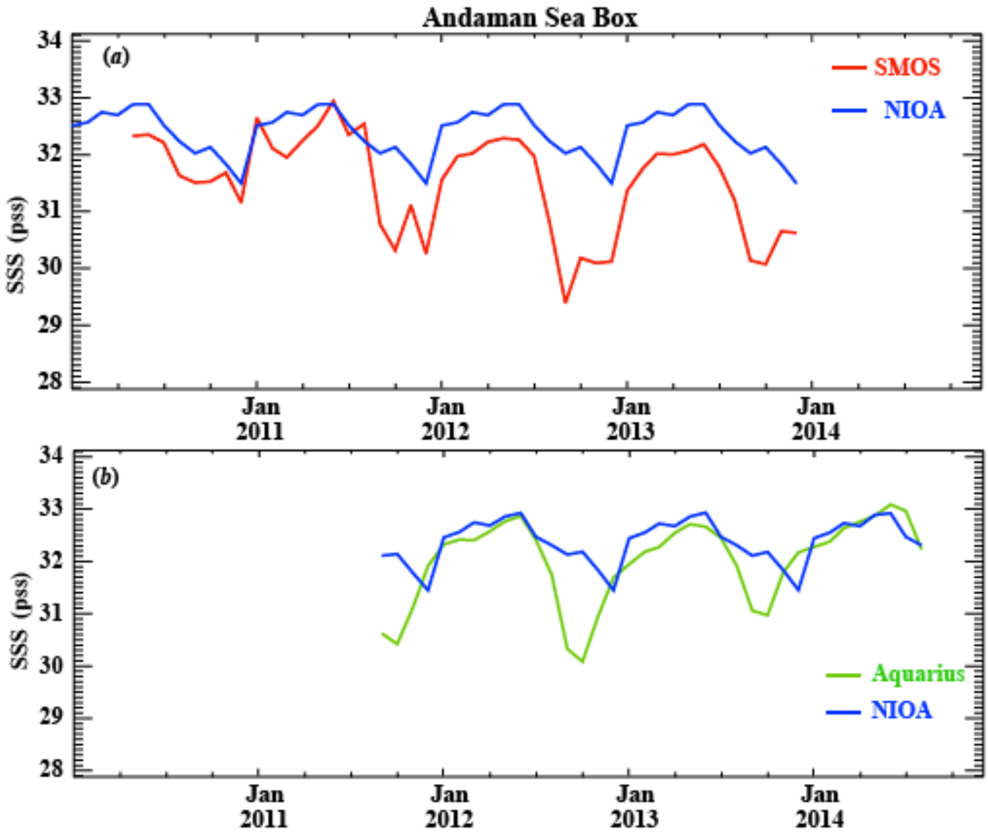
Andaman Sea Box
(a)
SMOS
NIOA
SSS (pss)
34
33
32
31
30
29
28
Jan 2011
Jan 2012
Jan 2013
Jan 2014
(b)
Aquarius
NIOA
SSS (pss)
34
33
32
31
30
29
28
Jan 2011
Jan 2012
Jan 2013
Jan 2014

Figure 13